computation

MDPI

Review

A Review on Computational Modeling Tools for MOF-Based Mixed Matrix Membranes

Seda Keskin [1,*] and Sacide Alsoy Altinkaya [2,*]

[1] Department of Chemical and Biological Engineering, Koç University, Rumelifeneri Yolu, Sariyer, 34450 Istanbul, Turkey

[2] Department of Chemical Engineering, İzmir Institute of Technology, Gülbahçe Campus, 35430 Urla, İzmir, Turkey

* Correspondence: skeskin@ku.edu.tr (S.K.); sacidealsoy@iyte.edu.tr (S.A.A.); Tel.: +90-212-3381362 (S.K.); +90-232-7506658 (S.A.A.); Fax: +90-212-3381548 (S.K.); +90-232-7506645 (S.A.A.)

Received: 31 May 2019; Accepted: 4 July 2019; Published: 18 July 2019



Abstract: Computational modeling of membrane materials is a rapidly growing field to investigate the properties of membrane materials beyond the limits of experimental techniques and to complement the experimental membrane studies by providing insights at the atomic-level. In this study, we first reviewed the fundamental approaches employed to describe the gas permeability/selectivity trade-off of polymer membranes and then addressed the great promise of mixed matrix membranes (MMMs) to overcome this trade-off. We then reviewed the current approaches for predicting the gas permeation through MMMs and specifically focused on MMMs composed of metal organic frameworks (MOFs). Computational tools such as atomically-detailed molecular simulations that can predict the gas separation performances of MOF-based MMMs prior to experimental investigation have been reviewed and the new computational methods that can provide information about the compatibility between the MOF and the polymer of the MMM have been discussed. We finally addressed the opportunities and challenges of using computational studies to analyze the barriers that must be overcome to advance the application of MOF-based membranes.

Keywords: trade-off; mixed matrix membrane; metal organic frameworks; computational tools; molecular simulation

1. Introduction

Membrane technology is a fast-growing technology for gas separation and has potential advantages in cost, energy efficiency and environmental impact compared to the traditional separation processes such as cryogenic distillation and absorption. An ideal gas separation membrane should have both high permeability and high selectivity to achieve the desired purity of the gas mixture with a small membrane area. Unfortunately, an upper-bound or trade-off between permeability and selectivity exists for various polymeric membranes and gas pairs as first reported by Robeson [1]. The upper-bound has been theoretically rationalized by different groups [2–10]. The predictions from the model developed by Freeman [2] suggested that membranes with a high fractional free volume but narrow free volume distribution are needed in order to exceed the upper-bound. Therefore, some of the recent studies focused on synthesizing new high free volume macromolecules with a well-controlled architecture [11]. Despite these efforts, improvement in the gas separation performance was found to be very little [12]. On the other hand, improved separation performance has been reported for the so-called mixed matrix membranes (MMMs), which contain a bulk continuous polymer phase and a dispersed inorganic particle phase [13]. Various conventional and new generation inorganic fillers such as zeolites, carbon molecular sieves and graphene have been added into different polymeric matrices [14]. Among

these porous fillers, metal organic frameworks (MOFs) have received special attention due to their well-defined structures and tunable pore sizes.

MOFs combine the properties of both inorganic and organic materials since they are assembled using metal ions with organic linkers [14]. The most important challenges involved in fabricating the MOF-based MMMs are to prevent the aggregation of the particles in the polymer and poor interaction between the particles and the polymer matrix. Rubbery polymers favor the formation of a defect-free interface between the particles and matrix due to their high degree of mobility. Flexible chains in the rubbery polymers make the membrane highly permeable, consequently, the gas transport is mainly dominated by the polymer matrix and the contribution of the MOF particles to the overall transport becomes very small. Glassy polymers have rigid chain structures, thus, they exhibit superior separation performance. On the other hand, the rigid structure weakens the interaction between polymers and particles. MOFs contain organic functionality in their bridging ligands, which can interact with the organic functionality in polymers. Numerous numbers of linkers and metal ions can be combined to fabricate MOFs, which can then be used as fillers in hundreds of different types of polymers; consequently, experimental screening of all MOF/polymer combinations is practically impossible. At this stage, computational tools play a key role in extensive screening of a large number of MOF/polymer combinations for particular gas separation. The MOF permeability obtained from the atomically detailed simulations is used as an input in permeation theories such as the Maxwell model to predict the gas permeabilities in MMMs. On the other hand, full atomistic simulations consider MOF and polymer simultaneously at the expense of more computational power requirements.

In this contribution, we review conventional computational methods that can be used for screening MOF/polymer combinations to design MMMs along with new computational algorithms used to determine the compatibility between the MOF and the polymer in the MMM.

2. Trade-Off between Permeability and Selectivity

Membrane technology is increasingly being used for applications such as hydrogen recovery, nitrogen generation and carbon dioxide removal due to its cost effectiveness and energy efficiency. An ideal membrane for a gas separation should have both high permeability and high selectivity. Higher permeability results in lower area to treat a given amount of gas, thereby decreasing the cost of the membrane unit while higher selectivity increases the purity of the product. Unfortunately, polymeric membranes exhibit a trade-off between permeability and selectivity, highly permeable membranes have low selectivity and vice versa.

Origin of the permeability/selectivity trade-off can be attributed to a broad distribution of free volume element sizes and relatively nonspecific interactions controlling the solubility of small molecules in polymers. To eliminate this trade-off, it is necessary to increase free volume element sizes while simultaneously narrowing the free volume element size distribution [15]. Isoporous membranes can have high permeability due to the lack of a tortuous pathway and high selectivity due to the uniform pore size distribution. Membranes produced from block copolymers usually have a very narrow pore size distribution however, block copolymers are expensive, thereby they cannot be potential candidates for a cost-effective manufacturing process. Many new glassy, high free volume polymers such as substituted polyacetylenes, perfluoropolymers, addition-type polynorbornene, polymers of intrinsic microporosity (PIMs), some polyimides and thermally rearranged polymers are being synthesized to improve permeability/selectivity trade-off [11]. The common feature of these polymers is to have rigid, twisted macromolecular backbones therefore, they cannot undergo large-scale conformational change.

3. Fundamental Approaches Employed to Describe Permeability and Perm-Selectivity Trade-Off

A general trade-off between permeability and selectivity was best described by the following equations:

$$\alpha_{ij} = \beta_{ij}/P_i^{\lambda_{ij}} \qquad \ln \alpha_{ij} = \ln \beta_{ij} - \lambda_{ij} P_i, \tag{1}$$

where α_{ij} and β_{ij} are empirical constants. To explain the theoretical basis of this equation, first the permeability and selectivity of gas separation membranes should be defined. Under the driving force of a pressure difference across a membrane, transport of gases through dense nonporous membranes is described by the solution diffusion mechanism. Based on this mechanism, the permeability coefficient of a polymer to gas species i, P_i , and the selectivity of a polymer (α_{ij}) for gas species i over j are defined as:

$$\begin{array}{c} P_i = D_i\, x\, S_i \qquad P_j = D_j\, x\, S_j \\ \alpha_{ij} = \frac{P_i}{P_j} = \left(\frac{S_i}{S_j}\right) x \left(\frac{D_i}{D_j}\right), \end{array} \tag{2}$$

where S_i is the solubility coefficient and D_{i} is the diffusion coefficient of gas species i. Different fundamental approaches have been offered to provide a general quantitative description of the upper bound performance of the polymeric membranes.

The first theoretical approach was proposed by Freeman [2] that considers the diffusion of gases as an activated process and describes the diffusivity based on the Arrhenius equation,

$$D_i = D_{oi} \exp\left(-\frac{E_{Di}}{RT}\right), \tag{3}$$

where D_{oi} is a front factor, E_{Di} is the activation energy for diffusion, R is the gas constant, and T is the absolute temperature. Activation energy is related to the front factor through a simple correlation [2],

$$\ln D_{oi} = a\frac{E_{Di}}{RT} - b, \tag{4}$$

where a has a universal value of 0.64 [2] and b has a value of 9.2 and 11.5 for rubbery and glassy polymers, respectively. Both a and b are independent of the gas type. The activation energy, E_{Di}, is modeled based on the penetrant size and penetrant jump length,

$$E_{Di} = cd_i^2 - f, \tag{5}$$

where d_i is the kinetic diameter of the penetrant and c and f are constants, which change with the polymer. Combining Equation (3) through (5) gives the following expression for the diffusion coefficient.

$$\ln D_i = -\left(\frac{1-a}{RT}\right) cd_i^2 + f\left(\frac{1-a}{RT}\right) - b. \tag{6}$$

The expression for the selectivity is then obtained by combining Equations (2) and (6):

$$\ln \alpha_{ij} = -\left[\left(\frac{d_j}{d_i}\right)^2 - 1\right] \ln P_i + \left\{\ln\left(\frac{S_i}{S_j}\right) - \left[\left(\frac{d_j}{d_i}\right)^2 - 1\right] x \left(b - f\left(\frac{1-a}{RT}\right) - \ln S_i\right)\right\}. \tag{7}$$

This equation has the same mathematical form as the empirical upper bond line given in Equation (1). Thus, empirical constants can be defined as follows:

$$\lambda_{ij} = \left(d_i/d_j\right)^2 - 1, \tag{8}$$

$$\beta_{ij} = \left(\frac{S_i}{S_j}\right) S_i^{\lambda_{ij}} \exp\left\{-\lambda_{ij}\left[b - f\left(\frac{1-a}{RT}\right)\right]\right\}. \tag{9}$$

Freeman's theory suggests that the most productive way to improve the permeability/selectivity properties is to modify the polymer's chemical structure in order to simultaneously increase the polymer backbone stiffness (i.e., increasing c value in Equation (6)) and interchain separation (i.e., increasing f value in Equation (6)). Both of these strategies result in an increase in the diffusivity and in the permeability. Robeson also noted that for many gas pairs, polymers that lie on or near the upper bound are amorphous with high glass transition temperature, rigid backbone and relatively

large interchain spacings. In this respect, it can be said that the qualitative predictions from the Freeman's theory are in agreement with the remarks made by Robeson [1]. Freeman's theory is restricted to light gases such as He, H_2, N_2, O_2, CO_2, CH_4, etc. This is because the theory neglects the polymer–penetrant interactions and assumes that the kinetic diameter of gases can be used as a measure of the penetrant size. Obviously, these assumptions are only valid for light gases. On the other hand, the theory has been extended to predict the upper bound for the separation of hydrocarbon pairs such as propylene/propane [3] and ethylene/ethane [4] and to predict the effect of temperature on the upper bound [5,6].

Alentiev and Yampolskii [7] used a simple free volume model to predict permeability and diffusivity of polymers:

$$D_i = F_i \exp\left(-\frac{V_i^*}{V_f}\right), \tag{10}$$

$$P_i = A_i \exp\left(\frac{B_i}{V_f}\right), \tag{11}$$

where V_f is the free volume, $V_i{}^*$ is a constant characteristic for the gas and F_i is a constant characteristic of the gas/polymer system. Based on the free volume theory, the expression derived for the selectivity is shown below:

$$\log \alpha_{ij} = -f + (1-g)\log D_i + \log\left(\frac{S_i}{S_j}\right), \tag{12}$$

$$f = \log F_j - \left(\frac{V_j^*}{V_i^*}\right)\log F_i, \tag{13}$$

$$g = \left(\frac{V_j^*}{V_i^*}\right). \tag{14}$$

Equation (12) has a similar mathematical form to Equation (7) derived by Freeman. It is noted that different approaches adopted by Yampolskii and Freeman result in the same recommendations for moving above the upper bound lines on the Robeson's plot. Simply, both theories indicate that solubility selectivity of the polymer/gas pairs should be improved in order to pass the upper bound line. Other theories based on Meares's cohesion energy density [8] and Sanchez–Lacombe's lattice fluid theory [9] have also been applied to interpret diffusivity and solubility upper bound, respectively. These theories have provided satisfactory results in describing the pure gas upper bounds. Obviously, they cannot be applied for gas mixtures especially in highly plasticizing environment such as CO_2. Lin and Yavari [10] extended the free volume theory to quantitatively describe the upper bounds for the mixed gas CO_2/CH_4 separations using polymeric membranes. The theory relates the reduction in glass transition temperature to the CO_2-induced plasticization effect. The predictions have shown that the intercept of the upper bound, β_{ij}, decreases with the increased CO_2 content in the mixture.

4. Mixed Matrix Membranes

Unlike polymeric materials, inorganic materials allow achieving narrow pore size distribution, hence they can provide an efficient solution to overcome the permeability/selectivity trade-off. In 1996, Koros and co-workers showed that the separation performance of carbon molecular sieve membranes was above the Robeson's upper bound [13]. Although the performance was improved, preparing large surface area, defect-free, ultrathin membranes of carbon molecular sieves and other inorganic materials are highly challenging. To overcome this limitation, a popular approach is to disperse these materials into a continuous polymeric matrix and resulting in a composite membrane structure, which is called a mixed matrix membrane (MMM). In designing MMM, compatibility between the filler and polymer, shape and size of the filler and homogeneous distribution of the filler should be carefully considered.

4.1. Types of Fillers Used

Fillers used in MMMs can be classified into two categories, such as spherical fillers with low aspect ratio and thin platelet type fillers with very high aspect ratio. During the past decades, different types of fillers have been used in designing MMM including zeolites, carbon molecular sieves, silica, metal oxide, carbon nanotube, layered silicate, metal organic framework and graphene. Among these fillers the most commonly used ones are zeolites, carbon molecular sieves and silica due to their well-defined structures.

Many groups reported advantages of using zeolites as a filler in a MMM to improve the permeability/selectivity trade-off for separation of different gas pairs [16–25]. The improvement in the separation performance of the membrane is based on the size and shape selectivity and specific sorption characteristics of zeolite. Simply, a gas component that can fit into the zeolite pores and/or having a higher affinity to the zeolite can permeate through the filler particle while the other components can travel around the zeolite particles through a more tortuous path. The research on the zeolitic fillers focused on choosing the appropriate dimension of the particle to separate gases with similar sizes and resolving the poor adhesion problem between the zeolite and polymer.

Carbon molecular sieves (CMS) in MMMs improve the trade-off problem through their size selectivity. CMS are produced from pyrolysis of mostly thermosetting polymers and their relatively wide opening with constricted apertures close to the molecular dimensions of the diffusing gas molecules can separate the gas molecules. Compared to zeolite particles, CMS have better affinity to glassy polymers and their synthesis conditions can be tailored to adjust the pore dimensions for separating a specific gas pair. The significant challenge in the synthesis of CMS is to prevent the formation of dead end pores. CMS-incorporated membranes have shown significant improvement in permeability/selectivity trade-off compared to that of the neat polymeric membranes [26–31].

Silica is also a commonly used inorganic filler in the MMM design. Different groups reported an improvement in gas permeability upon adding silica particles into polymer matrixes [32–36]. The increase in permeability was attributed to the improved gas solubility as a result of the interaction between the residual silanol groups of the silica domain and polar gases and the increase in the mean distance between the polymer chains through the reduction of the polymer chain packing density at the interface between the two phases. Metal oxide nanoparticles such as MgO and TiO_2 are also added as alternative inorganic fillers into polymers. High specific area of the metal oxides with their nanoscale sizes allows homogeneous distribution and non-selective void formation at the polymer/nanoparticle interface [14]. Adding MgO into membranes resulted in an improvement in the permeability, which was ascribed to either enhanced gas diffusivity [37] or enhanced solubility [38] depending on the gas pair to be separated.

In addition to the conventional fillers, zeolite, CMS, silica and metal oxides, new alternative fillers with controllable cage dimensions are being explored. Carbon nanotubes (CNT) are considered as one of the new generation fillers. The extensive usage of the CNT has started after the theoretical work by Sholl and co-workers [39,40]. They have reported that the transport of small gases such as H_2 and CH_4 is orders of magnitude faster in CNT than the one in zeolite or other inorganic nanoporous materials. Unfortunately, experimental results did not support these theoretical predictions [41–48]. This can be attributed to the difficulty in dispersing CNT due to the tendency of stabilized bundle formation, difficulty in achieving vertical alignment of tubes in addition to the poor adhesion between the CNT and polymer matrix. Recent application of clay in the MMM has been demonstrated [49,50]. An important advantage of clay as a filler is its aspect ratio as high as 1000 due to the ability of the silicate particles to disperse into individual layers. This simply requires expanding the interlayer space of the clay through chemical modification. Similar to clay, graphite has also a very high aspect ratio, thereby, is considered as a promising filler in MMM. Different groups incorporated graphene oxide (GO) nanosheets into polymers to improve the gas separation performance [51–55]. Two dimensional (2D) graphene nanosheets in MMM form sub-nanometer channels between the sheets allowing size based separation. Size-selectivity depends on engineering the nanochannels between GO nanosheets

by controlled reduction or cross-linking to achieve targeted separation. Beside graphene, other promising porous fillers are MOFs. The usage of MOFs in designing novel MMM will be reviewed in the following sections.

4.2. Fundamental Approaches for Predicting Permeation through MMMs

Permeation models through MMMs are usually based on theories developed for thermal/electrical conduction of heterogeneous media due to the analogy between permeation and conduction through composite materials. Three approaches have been used for modeling permeation through MMMs: The resistance-based models, effective-medium theory-based models and simulation-based rigorous models (Figure 1).

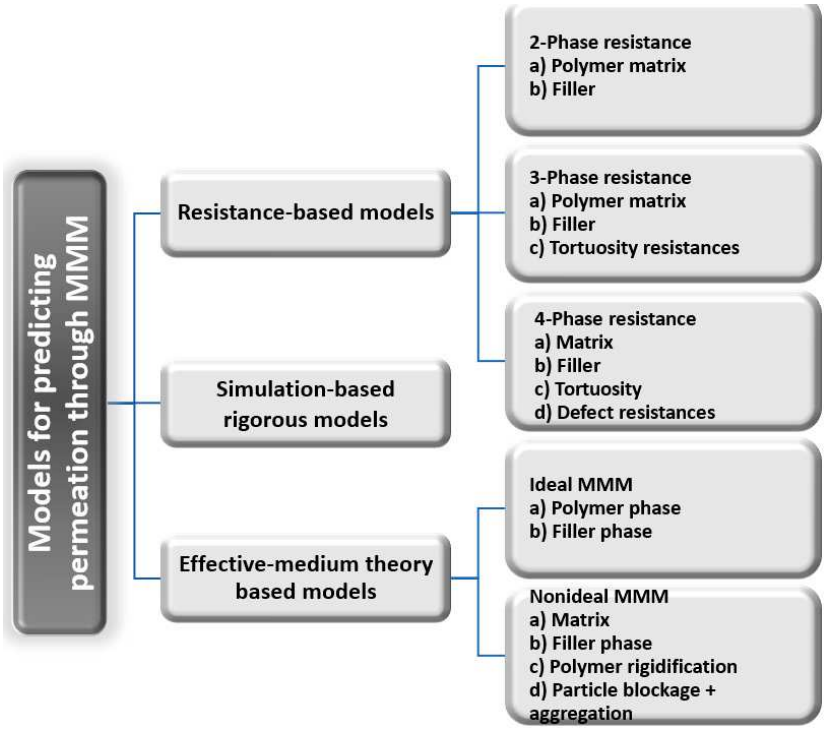


Figure 1. Models commonly used for predicting permeability of gases in mixed matrix membranes (MMMs).

In resistance model approach (RMA), MMM is visualized as a two-phase composite containing multiple sheets of polymer and filler alternated in series or in parallel to the flow direction [56]. The series model gives the lower limit while the parallel model predicts the upper limit for the permeability in an ideal MMM. More complex models including additional diffusional resistance due to tortuosity effects have also been developed [57–60] and they are listed in Table 1.

In the effective medium approach (EMA), permeability is generally predicted based on the volume fraction of the filler in the MMM and permeabilities of each constituent in the structure [61]. The models based on effective medium approach consider random distribution of spherical fillers [62–65] while most RMA models assume regular distribution of platelet or cubic particles [66–68]. EMA models are classified into two categories (Table 2): Models following the Maxwell's theory [63,69–75] and those following the Bruggeman's theory [61,62,73,76]. The Maxwell model was originally developed to calculate the electrical conductivity of infinitely diluted cluster of particles embedded in an infinite matrix [69]. The Maxwell model can only be applied for low filler loading since it does not consider interaction between the particles. The model is based on two-phase morphology, thus it predicts permeabilities for an ideal MMM (Figure 2). Based on the Maxwell theory, several models (Table 2) have been developed to account for the permeation in high filler loaded composites [62], non-ideal

polymer–particle interface [72] and to accommodate both the partial pore blockage and polymer rigidification and particle aggregation [75] (Figure 3). The Bruggeman's theory was adapted from an expression derived for the dielectric permeability of the dispersed composites and it is applicable to moderate filler loadings (≤0.35) [61]. The theory assumes that the composite is formed by incrementally adding new dispersed phase to an existing composite. The main assumption in the theory is that newly added particles are dilute therefore, they only interact with those previously added to the composite. The Bruggeman's model has also been extended to take into account a voided or rigidified interfacial region at the filler particle surface [76].

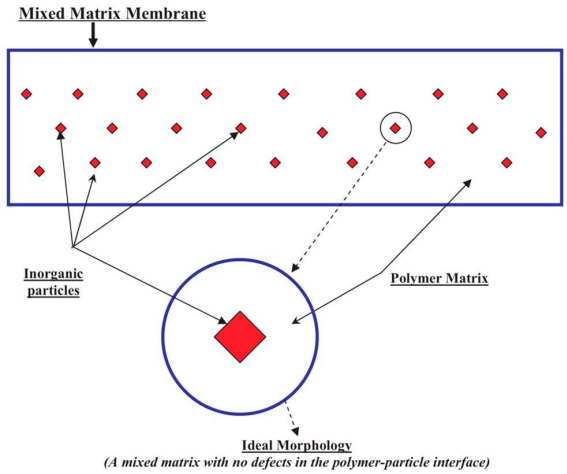


Figure 2. Schematic diagram of ideal MMM structure. Reproduced with permission from Ref. [77] Copyright 2010 Elsevier.

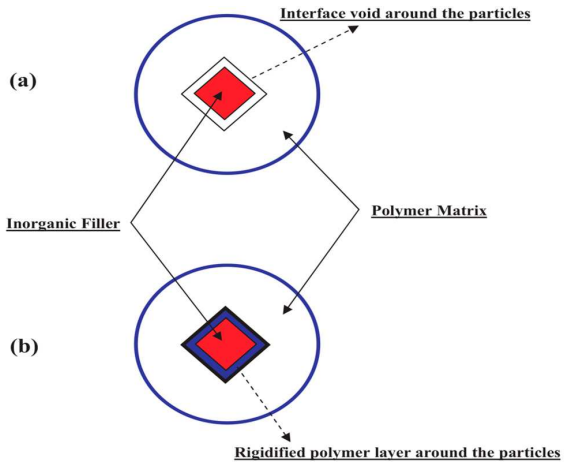


Figure 3. Schematic diagram of non-ideal MMM morphologies. Interface void (**a**) and rigidified polymer layer (**b**) in the polymer–particles interface. Reproduced with permission from Ref. [77] Copyright 2010 Elsevier.

In the simulation-based rigorous modeling approach, the transport through the MMM is solved numerically. The MMM permeability is predicted using single-gas experimental or simulation-based adsorption and permeation data on the individual MMM materials. Using the simulation approach, complexities such as the effect of filler size, shape, nonlinear sorption isotherm and membrane geometry can be easily taken into account. However, the numerical solution of coupled partial differential equations requires advanced methods such as the finite-element, finite difference or boundary volume methods and this limits the practical use of the method in predicting the permeabilities. Studies implementing simulation-based rigorous modeling approach can be found in a recent review [78]. The models listed in Tables 1 and 2 are used to predict the permeability in MMMs by using

the experimentally measured permeabilities of filler and continuous phases. Figure 4 compares permeabilities and selectivities predicted from different models with the experimental permeation data of CO_2 and CH_4 in CMS/Matrimid MMM [73]. In the graph the "Present Model" refers to the "Pseudo-two phase Pal model" in Table 2. The results have shown that the best prediction with the least percentage average absolute relative error was obtained with the pseudo-two phase Pal model. This simply indicates the importance of including presence of voids in the predictions. Monsalve-Bravo and Bhatia [79] (MB-B) extended the Chiew and Glandt model in Table 2 by taking into account both the particle size and isotherm nonlinearity. Figure 5 illustrates that the prediction from this model (MB-B model) resulted in the smallest deviation from the experimental data for O_2 and N_2 permeabilities in CMS/Ultem MMM, however, the permeabilities should be evaluated using numerical methods [73].

Among existing models, the Maxwell model is commonly used to predict permeabilities in MMM. However, the predictive ability of this model is poor since it does not take into account the effect of particle size distribution, the shape and aggregation of particles and other defects in the structure. Unfortunately, preparing MMMs with no defects is highly challenging due to the incompatibility between filler and matrix as well as the difficulty in achieving uniform distribution of filler through the matrix structure. Although models have been developed to consider interfacial defects, they are based on empirical fitting parameters such as interfacial layer thickness. Thus, new theoretical models are needed to take into account the following issues: (1) Particle size, size distribution, particle pore size and its distribution, shape, inhomogeneity and aggregation of particles, (2) nonlinear sorption isotherm, (3) nonlinear concentration profile and non-uniform permeabilities across the MMM, (4) operating conditions such as temperature, pressure and gas feed composition. In addition, the input parameters needed for predicting the permeabilities should be measured or characterized in advance so that permeability data for MMMs should not be needed to estimate these parameters.

Table 1. Resistance-based models.

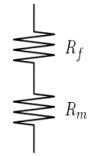
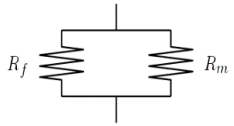
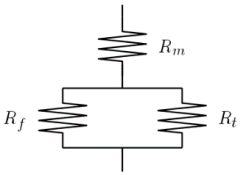
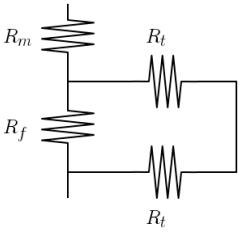
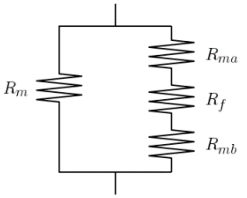
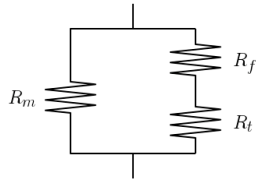
Reference	Key Assumptions	Permeability	Resistance Circuit
Zimmerman et al. [56]	Two resistances: Matrix and filler	$P_{eff} = \frac{P_m P_f}{P_m \varphi_f + P_f (1-\varphi_f)}$	
Zimmerman et al. [56]	Two resistances: Matrix and filler	$P_{eff} = P_f \varphi_f + P_m (1-\varphi_f)$	
Te Hennepe et al. [57]	One-dimensional transport, idealized MMM as a lamella containing composite layers. Polymer region is assumed in series with parallel resistances of the second mixed region. Polymer, filler and diffusional resistance to account for tortuosity effects in the permeant diffusion path are considered.	$P_{eff} = P_m \left[\left(1-\varphi_f^{\frac{1}{3}}\right) + \frac{\frac{3}{2}\varphi_f^{\frac{1}{3}} P_m}{P_m (1-\varphi_f) + \frac{3}{2} P_f \varphi_f} \right]^{-1}$	
Cussler [58]	Idealize membrane as lamella. Each lamella contains two layers. Pure polymer and polymer and filler. Resistance of pure polymer is connected in series with the parallel resistances due to filler and tortuosity in the second mixed lamella layer. Two-dimensional transport in the mixed region is assumed to be in the permeation direction through filler and perpendicular to the permeation direction through polymer.	$P_{eff} = P_m \left[\left(1-\varphi_f\right) + \left(\frac{P_f}{\varphi_f P_m} + \frac{4(1-\varphi_f)}{\lambda_f^2 \varphi_f^2} \right)^{-1} \right]^{-1}$	
Ebneyamini et al. [59]	Suggested for ideal MMM containing cubic fillers. MMM four: (1) The continuous phase above the filler, (2) the cubical filler particle located in the centre of the unit element, (3) the continuous phase below the filler and (4) the continuous phase, which surrounds Regions 1, 2 and 3. The model is based on thee resistances of these four regions.	$P_{eff} = \tau \left[\left(1-{\varphi_f}^{2/3}\right) P_m + \frac{P_m P_f {\varphi_f}^{2/3}}{{\varphi_f}^{1/3} P_m + \left(1-{\varphi_f}^{1/3}\right) P_f} \right]$	

Table 1. *Cont.*

Reference	Key Assumptions	Permeability	Resistance Circuit
Kang et al. [60] *	Developed for MMM containing a nano-sized tubular filler. Matrix and filler resistances are assumed to be serially connected. The effect of orientation of the filler with respect to the permeation direction was considered through an arbitrary filler orientation distribution function.	$P_{eff}^{Oriented} = P_c\left[\begin{array}{c}\left(1-\frac{\cos\theta}{\cos\theta+\lambda_f\sin\theta}\varphi_f\right)+\\ \frac{P_m}{P_f}\left(\frac{1}{\cos\theta+\lambda_f\sin\theta}\right)\varphi_f\end{array}\right]^{-1}$ $P_{eff}^{Random} = \frac{\pi}{2}P_m\left[\int_0^{\frac{\pi}{2}}\frac{P_c}{P_{eff}^{Oriented}(\theta)}d\theta\right]^{-1}$	

f: Filler; m: Matrix (dispersed) phase; P: Permeability; θ: Orientation of the filler with respect to the permeation direction; φ: Volume fraction; τ: Empirical correction factor to account for tortuosity effect; λ_f: Aspect ratio of the filler (flake); R_m: Resistance of the matrix phase; R_f: Resistance of the filler phase; R_t: Resistance due to transport around the fillers; R_{ma}: Resistance of the matrix phase above the filler; R_{mb}: Resistance of the matrix phase below the filler; *: Definitions of the resistances are different for the cases of random and oriented fillers.

Table 2. Effective medium theory-based models.

Reference	Key Assumptions	Permeability	Applicable Range of the Model (Volume Fraction of Filler)
Maxwell theory [69]	Dispersion in the matrix is spherical. No interaction between the particles	$P_{eff} = P_m\left[\frac{1+2\beta_{fc}\varphi_f}{1-\beta_{fc}\varphi_f}\right] = P_m\left[\frac{P_f+2P_m-2\varphi_f(P_m-P_f)}{P_f+2P_m+\varphi_f(P_m-P_f)}\right]$ $\beta_{fm} = (\alpha_{fm}-1)/(\alpha_{fm}+2)\alpha_{fm} = P_f/P_m$	<0.2
Maxwell-Wagner–Sillars model [70]	Dispersion in the matrix is ellipsoid. No interaction between the particles	$P_{eff} = P_m\left[\frac{\sigma_f P_f+(1-\sigma_f)P_m-(1-\sigma_f)\varphi_f(P_m-P_f)}{\sigma_f P_f+(1-\sigma_f)P_m+\sigma_f\varphi_f(P_m-P_f)}\right]$	<0.2
Chiew and Glandt [63]	Dispersion of spherical particles in the matrix is modeled using pair-correlation functions of hard-sphere fluid simulations.	$P_{eff} = P_m\left[\frac{1+2\beta_{fm}\varphi_f+\left(K_2-3\beta_{fm}^2\right)\phi_f^2}{1-\beta_{fm}\varphi_f}\right]$ $K_2 = a+b\varphi_f^{\frac{3}{2}}$ $a = -0.002254-0.123112\beta_{fm}+2.93656\beta_{fm}^2+1.6904\beta_{fm}^3$ $b = 0.0039298-0.803494\beta_{fm}-2.16207\beta_{fm}^2+6.48296\beta_{fm}^3+5.27196\beta_{fm}^4$	<0.645
Lewis-Nielsen [71]	Dispersion in the matrix is spherical. Loose or random close packing of spheres and morphology of particles are considered with the maximum achievable volume fraction (φ_m) of filler.	$P_{eff} = P_m\left[\frac{1+2\beta_{fm}\varphi_f}{1-\beta_{fm}\varphi_f\psi_m}\right]$ $\psi_m = 1+\left[(1-\varphi_m)/\varphi_m^2\right]\varphi_f$	$<\varphi_m$ φ_m: 059 (Loose random packing) φ_m: 0.64 (Close random packing φ_m: 0.86 (Binary packing of spherical particles)
Felske model [72]	Accounts for non-ideal polymer–particle morphologies. Core-shell particles are assumed to be non-interactive.	$P_{eff} = P_m\left[\frac{2(1-\varphi_f)+(1+2\varphi_f)(\eta/\gamma)}{(2+\varphi_{fi})+(1-\varphi_f)(\eta/\gamma)}\right]$ $\eta = (2+\delta^3)\alpha_{fm}-2(1-\delta^3)\alpha_{im}\delta = \frac{l_i+r_f}{r_f}\alpha_{im} = P_i/P_c$ $\gamma = (1+\delta^3)-(1-\delta^3)\alpha_{fi}\alpha_{fi} = P_f/P_i$ $\varphi_{fi} = \frac{\varphi_f^N}{\varphi_f^N+\left[\left(1-\varphi_f^N\right)/\delta^3\right]}$	<0.2

Table 2. *Cont.*

Reference	Key Assumptions	Permeability	Applicable Range of the Model (Volume Fraction of Filler)
Modified Felske model [73]	Accounts for the morphology and packing intensity of particles.	$P_{eff} = P_m\left[\frac{1+2[(\eta-\gamma')/(\eta+2\gamma')]\varphi_f}{1-[(\eta-\gamma')/(\eta+2\gamma')]\psi_m\varphi_f}\right]$	<0.2
Two-Phase Maxwell model [74]	Three-phase composite can be idealized as pseudo two-phase composite (Phase 1: Polymer matrix, Phase 2: Combined filler-interface)	$P_{eff} = P_m\left[\frac{P^f_{eff}+2P_m-2\varphi_{fi}\left(P_m-P^f_{eff}\right)}{P^f_{eff}+2P_m+\varphi_{fi}\left(P_m-P^f_{eff}\right)}\right]$ $P^f_{eff} = P_i\left[\frac{P_f+2P_i-2\varphi_s\left(P_i-P_f\right)}{P_f+2P_i+\varphi_s\left(P_i-P_f\right)}\right]$ $\varphi_s = 1/\left(1+l_i/r_f\right)^3$	<0.2
Four-Phase Maxwell model [75]	The model considers chain rigidification, pore blockage effect and particle aggregation. Permeability is modeled using four phases: Phase 1: Polymer matrix, Phase 2: Chain rigidification region, Phase 3: Nanoparticles and particle blockage layer, Phase 4: Particle aggregate layer	$P_{eff} = P_m\left[\frac{P_{deff}+2P_m-2\left(\varphi_f+\varphi_{blo}+\varphi_{rig}\right)\left(P_m-P_{deff}\right)}{P_{deff}+2P_m-\left(\varphi_f+\varphi_{blo}+\varphi_{rig}\right)\left(P_{rig}-P_{deff}\right)}\right]$ $P_{deff} = P_{4eff}\xi + P_{2eff}(1-\xi)$ $P_{2eff} = P_{rig}\left[\frac{P_{3eff}+2P_{rig}-2\varphi_2\left(P_{rig}-P_{3eff}\right)}{P_{3eff}+2P_{rig}+\varphi_2\left(P_{rig}-P_{3eff}\right)}\right]$ $\varphi_2 = \frac{\left(r_f+l_{blo}\right)^3}{\left(r_f+l_{blo}+l_{rig}\right)^3}$ $P_{3eff} = P_{blo}\left[\frac{P_f+2P_{blo}-2\varphi_3\left(P_{blo}-P_f\right)}{P_f+2P_{blo}+\varphi_3\left(P_{blo}-P_f\right)}\right]$ $\varphi_3 = \frac{r_f^3}{\left(r_f+l_{blo}\right)^3}$	<0.2
Bruggeman [61]	Composite is formed by incrementally adding new dispersed phase to an existing composite. Newly added particles do not interact with each other, they only interact with those previously added to the composite.	$\left[\frac{P_{eff}}{P_m}\right]^{\frac{1}{3}}\left[\frac{\alpha_{fm}-1}{\alpha_{fm}-\left(P_{eff}/P_m\right)}\right] = \left[1-\varphi_f\right]^{-1}$	<0.35
Pal [62]	Composite with a high filler loading is obtained by successively adding small differential quantities of particles to the system until the desired loading is achieved.	$\left[\frac{P_{eff}}{P_m}\right]^{\frac{1}{3}}\left[\frac{\alpha_{fm}-1}{\alpha_{fm}-\left(P_{eff}/P_m\right)}\right] = \left[1-\frac{\varphi_f}{\varphi_m}\right]^{-\varphi_m}$	$<\varphi_m$

Table 2. *Cont.*

Reference	Key Assumptions	Permeability	Applicable Range of the Model (Volume Fraction of Filler)
Pseudo-two phase Bruggeman model [76]	The model considers voids creation in the interface layer of MMM. The MMM is assumed to consist of the pseudo two-phase region: The matrix and the filler + void volume region.	$\left[\frac{P_{eff}}{P_m}\right]^{\frac{1}{3}}\left[\frac{\left(P^f_{eff}/P_m\right)-1}{\left(P^f_{eff}/P_m\right)-\left(P_{eff}/P_m\right)}\right]=\left[1-\varphi_{fi}\right]^{-1}$ $\left[P^f_{eff}/P_i\right]^{\frac{2}{3}}=1-\varphi_s P_f << P_i$ $\left[\frac{P_{eff}}{P_i}\right]^{\frac{1}{3}}\left[\frac{(P_f/P_i)-1}{(P_f/P_i)-\left(P^f_{eff}/P_i\right)}\right]=[1-\varphi_s]^{-1}P_f \geq P_i$	<0.35
Pseudo-two phase Pal model [73]	Polymer matrix and Interfacial rigidified matrix chains are considered in predicting the permeability.	$\left[\frac{P_{eff}}{P_m}\right]^{\frac{1}{3}}\left[\frac{\left(P^f_{eff}/P_m\right)-1}{\left(P^f_{eff}/P_m\right)-\left(P_{eff}/P_m\right)}\right]=\left[1-\frac{\varphi_{fi}}{\varphi_m}\right]^{-\varphi_m}$ $\left[\frac{P^f_{eff}}{P_i}\right]^{\frac{1}{3}}\left[\frac{(P_f/P_i)-1}{(P_f/P_i)-\left(P^f_{eff}/P_i\right)}\right]=\left[1-\frac{\varphi_s}{\varphi_m}\right]^{-\varphi_m}$	$<\varphi_m$

f: Filler; m: Matrix (dispersed) phase; i: Interfacial shell around the filler phase; *blo*: Pore blockage layer; *rig*: Rigidified polymer region; P: Permeability; φ: Volume fraction; σ_f: Particle shape factor; φ_m: Maximum packing volume fraction of filler particles; φ_f^N: The nominal filler volume fraction; r_f: Core radius of the dispersed phase particle (radius of the particle); l: Thickness; ξ: The partial fraction of particle aggregation.

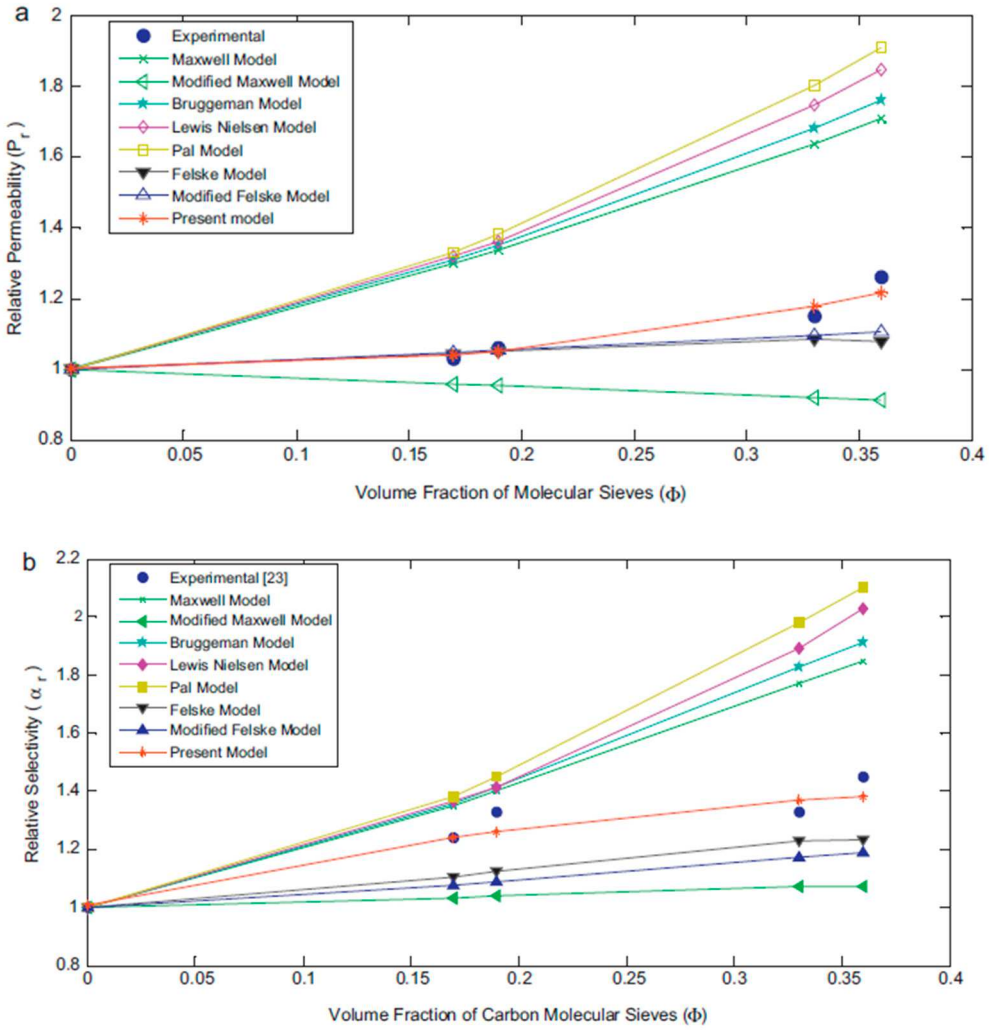


Figure 4. Comparison of the theoretical (**a**) permeability and (**b**) selectivity predicted from different models with the experimental data of CO_2 and CH_4 in carbon molecule sieves (CMS)/Matrimid MMM. Reproduced with permission from Ref. [73] Copyright 2011 Elsevier.

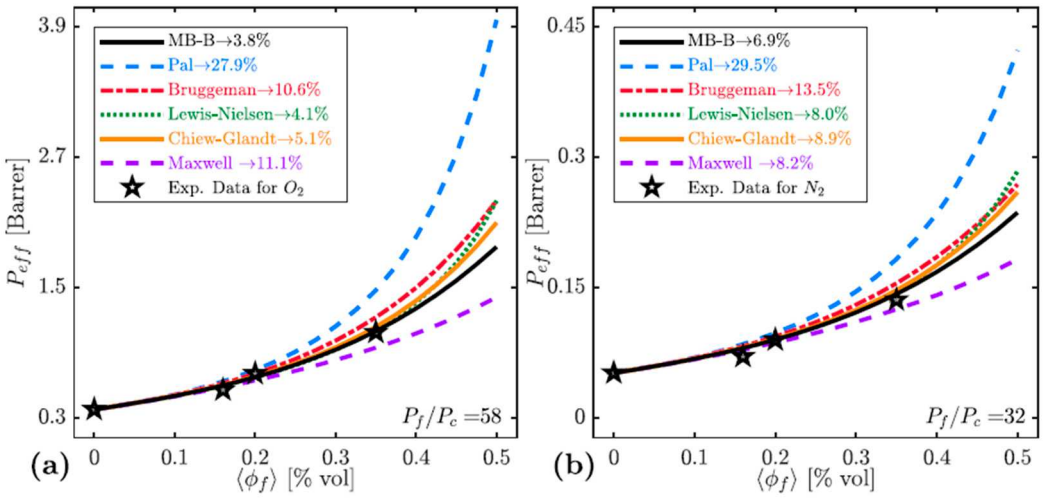


Figure 5. Comparison of experimental and theoretical (**a**) O_2 (**b**) N_2 permeabilities predicted from different effective medium theory based models for CMS/Ultem MMM. Adapted from Ref. [78].

5. Recent Advances in Metal Organic Framework (MOF)-Based MMMs for Gas Separations

MOF-based MMMs offer several advantages over traditional MMMs in which other types of porous materials are used as fillers. For example, the pore structure of MOFs can be tailored to achieve a target gas separation and MOFs have organic linkers, which generally lead to a good compatibility with the polymeric matrix. On the other hand, there are still several technical challenges related with the development of MOF-based MMMs such as pair-wise selection of MOF and polymer, stability and dispersion of MOF in the polymer matrix, existence of the interfacial defects in the MMM. A recent review article summarized these issues together with the possible strategies to improve the compatibility between the filler and polymer using different experimental approaches [80]. In this section, we will specifically focus on a recent advancement in the field of MOF-based MMMs, incorporation of ionic liquids (ILs) as interface agents into the MOF/polymer MMMs to improve filler/polymer interfacial defects and to enhance the gas separation performance of MMMs. The idea here is that ILs, which are molten salts at room temperature with good thermal and electrochemical stability, low volatility and high CO_2 solubility [81,82], can act like a wetting agent and the presence of ILs can eliminate the non-selective defects in the MMM. For example, a zeolitic imidazolate framework (ZIF-8) was incorporated into a miscible IL blend system composed of a polymerizable room-temperature IL (poly(RTIL)) and free room-temperature ILs (RTILs) [83]. Experimental results demonstrated that free RTILs are miscible with poly(RTIL), while ZIF-8 are uniformly dispersed in the MMMs. It was reported that introduction of ZIF-8 enhanced the membrane's gas permeability without compromising the CO_2/N_2 and CO_2/CH_4 selectivities, which indicated the absence of defects in the MMM. Li et al. [84] introduced a novel strategy to develop toughened MOF-polymer interface by confining a RTIL into ZIF-8 pores. Rather than dispersing free ILs and MOFs directly into the polymer as shown in Figure 6a, they incorporated ILs into MOFs as represented in Figure 6b. IL@ZIF-8/Pebax membranes were reported to have better molecular sieving properties compared to ZIF-8/Pebax membranes due to the strong hydrophobic–hydrophobic interaction between ZIF-8 and polyamide block of the polymer and because of the decrease in the effective aperture size of ZIF-8. Both the tensile strength and elongation of IL@ZIF-8/Pebax membranes were reported to increase with the increased loading of IL@ZIF-8. IL@ZIF-8 MMMs also displayed a substantial improvement in the CO_2 permeability, CO_2/N_2 and CO_2/CH_4 selectivities compared to pristine Pebax.

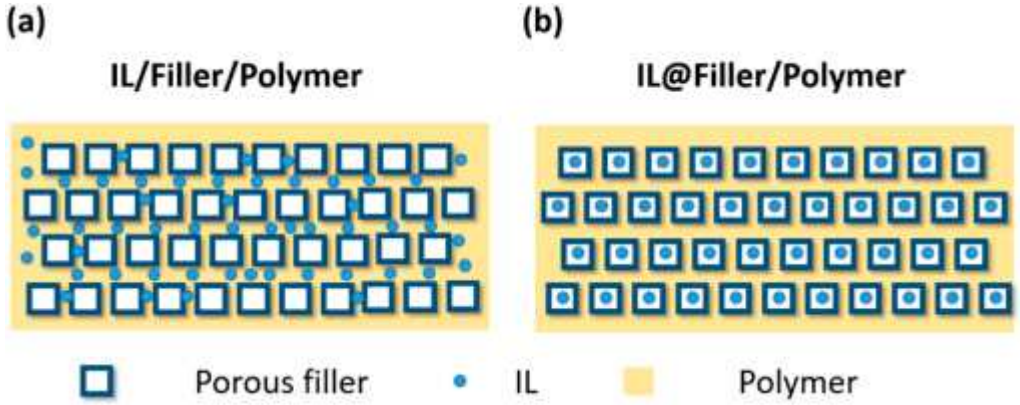


Figure 6. Structures of MMMs with ionic liquid (IL) and porous metal organic framework (MOF) fillers: (**a**) Free IL dispersed in filler/polymer matrix, (**b**) IL confined in the porous MOF fillers. Reprinted from Ref. [84] with permission from Elsevier.

Ban et al. [85] confined an imidazolium-based IL into the cages of ZIF-8 by in-situ ionothermal synthesis in order to tailor the effective cage size of ZIF-8 to be between the kinetic diameters of CO_2 and N_2 molecules. IL@ZIF-8 MMMs were reported to show high permeability and selectivity that can exceed the upper bound of polymeric membranes both for CO_2/N_2 and CO_2/CH_4 separations and excellent long-term stability of the membranes was shown. This work highlighted that RTILs can be

used as cavity occupants in order to change the microenvironment of MOF nano-cages. Extension of this concept to other types of MOFs and ILs to achieve a controllable change in the pore size of MOFs can be possible by the appropriate selection of ILs with proper chain length for a gas separation process based on the molecular-sieving mechanism.

ILs are not only used to change the pore size of narrow-pored MOFs such as ZIF-8 but also embedded into large-pored MOFs such as CuBTC (also known as HKUST-1). The group of Zhu [86] fabricated a thin layer of IL which acted as the HKUST-1/polymer interfacial binder to improve the adhesion between the micron-sized HKUST-1 and polymer. They reported that >90 vol% of interfacial voids in the MMM were eliminated by the IL incorporation due to the favorable MOF/IL and IL/polymer interactions that facilitate the enhancement of MOF/polymer affinity. Both the CO_2 permeability and CO_2/CH_4 selectivity were enhanced by embedding HKUST-IL filler into the polymer. This study showed that IL incorporation can be a good strategy to improve the compatibility between the large-pored MOF and polymer and gas separation efficiency of the MMM. Expansion of this type of studies on different combinations of ILs, MOFs and polymers will provide very useful guidelines for the rational design and development of IL@MOF/polymer MMMs having the desired interfacial properties. We note that IL/MOF/polymer and IL@MOF/polymer MMMs that we reviewed above were experimentally investigated. There is a huge potential for the computational modeling of MMMs that are composed of ILs, MOFs and polymers since there are theoretically infinite number of combinations of these materials and it is simply not possible to identify the most appropriate combination for a MMM using a purely experimental approach. Computational modeling studies can provide atomistic-level insights into the IL-MOF, IL-polymer and MOF-polymer interactions and even predict the best combinations of the three components to achieve a high performance MMM.

6. Computational Tools in High-Throughput Screening of MOF for MMM Applications

One of the biggest challenges of designing MOF-based MMMs is the very large number of available MOFs. Although the existence of very large number and variety of materials seem to be a great opportunity for the researchers, it is in fact very difficult to select the most suitable MOF filler for a given polymer and for a target gas separation process. Considering the fact that there are hundreds of different types of polymers and several thousands of MOFs, it is not practical to experimentally test all possible combinations of MOF/polymer MMMs. At that point, the importance of the computational studies, which can provide information about the predicted gas permeability and selectivity of MOF/polymer MMMs has emerged. Results of computational studies can be used to guide the experimental efforts, time and resources to the most promising MOF/polymer pairs. Mathematical description of gas transport through a MMM is complex. There are currently two approaches in the literature to computationally model the gas separation performances of MOF/polymer MMMs and we briefly discussed these approaches below.

In the first approach, atomically detailed simulations are utilized to obtain the gas permeability data of MOFs due to the limited experimental permeability data of MOFs in the literature. This data is then combined with the experimental gas permeability data of polymers using a theoretical permeation model as we discuss above to predict the gas permeability of MOF/polymer MMMs. Grand canonical Monte Carlo (GCMC) simulations are used to compute gas adsorption and molecular dynamics (MD) simulations are used to calculate gas diffusion in the pores of MOFs. The details of this approach and the details of molecular simulations of MOFs can be found in several review articles in the literature [87–92]. Briefly, GCMC simulations mimic the experimental gas uptake of a porous material at a predefined pressure and temperature whereas MD simulations are used to compute the diffusion rate of the adsorbed gas in the pores of the material. Generally, a GCMC simulation is first performed to calculate the number of adsorbed gas molecules in a MOF material, followed by an MD simulation in which the result of the GCMC simulation is the input of the MD simulation. The adsorption and diffusion data obtained from these simulations is then combined to compute the gas flux (J) of a MOF using the Fick's law, $J = -D_t(c) \cdot \nabla c$, where $D_t(c)$ represents the transport diffusivity computed from

MD and ∇c is the concentration gradient computed from the GCMC simulation. The gas flux can be then converted to permeability using the pressure drop (Δp) and membrane thickness, L as follows: $P = J/\Delta p/L$.

A summary of the computationally studied MOF/polymer MMMs was provided in the literature by giving the names of the MOF and polymer, type and conditions of the gas separation process studied using the MMM, the name of the theoretical permeation models used and the corresponding references [89]. Keskin's group widely used this approach [93–100] by first validating the accuracy of molecular simulations by comparing the simulated gas permeability data of MOF-based MMMs with the available experimental data and then predicting the gas permeabilities of MOF-based MMMs for which experimental data was not available. As an example, Figure 7 shows the good agreement between simulated CO_2, H_2, CH_4 and N_2 permeabilities and the experimentally measured gas permeabilities of 18 different types of MOF and ZIF-based MMMs. Molecular simulations, GCMC and MD as described above, were performed for MOFs under the same pressure and temperature with the experiments that reported gas permeabilities of MOF/polymer MMMs. Both the modified Felske model and the Maxwell model were used to predict the gas permeabilities. Molecular simulations assume perfect-defect free MOFs in contrast to experiments and generic force fields are used in molecular simulations, which does not account for the special interactions between the different components of MMM. As a result, there are some differences between the experimentally measured and computed gas permeabilities. The results of Keskin and Erucar [90] showed that computational methods could be used to make reasonably accurate predictions for the gas permeability of MOF-based MMMs especially at low volume fractions of the MOF fillers. It is important to note that this approach predicts the gas separation performance of the MMMs assuming perfect adhesion and compatibility between the MOF filler and polymer matrix and it only describes the MOF particle at the atomistic-level, not the polymer. Therefore, this approach is not able to provide a whole atomistic view of the MMM.

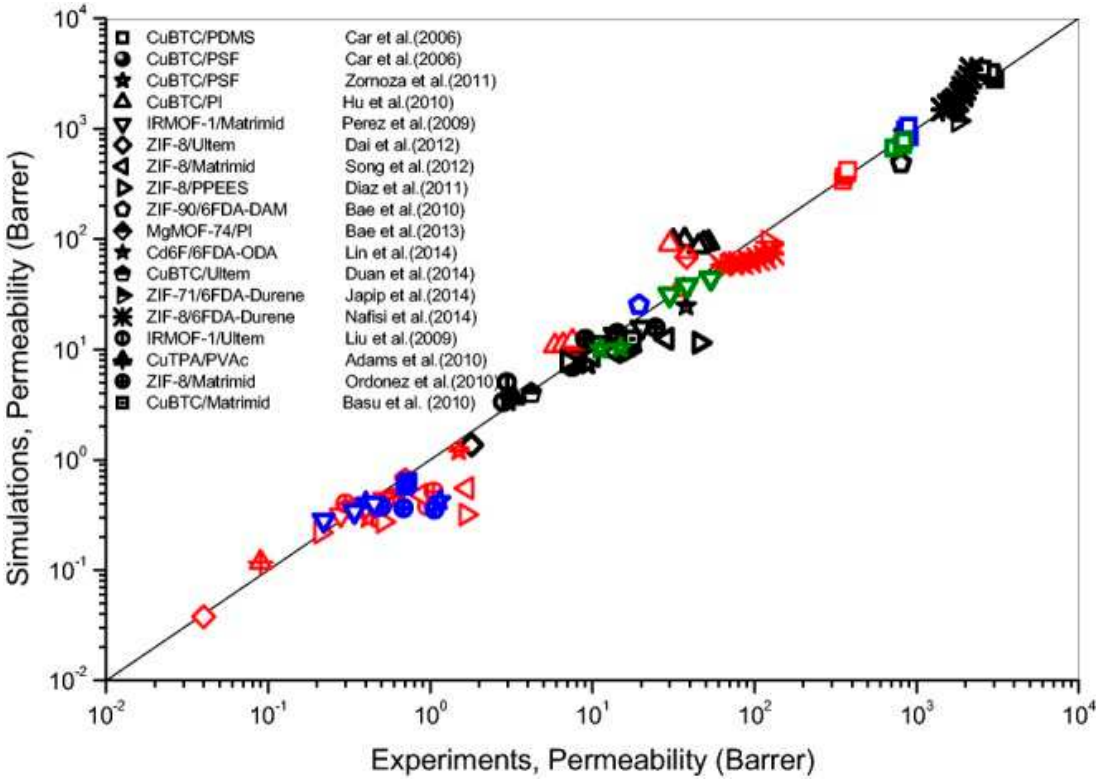


Figure 7. Comparison of our molecular simulation results with experimentally measured H_2 (green), CH_4 (blue), CO_2 (black) and N_2 (red) permeability of MOF-based MMMs. Reprinted from ref. [90] with permission from Wiley.

The second approach for computational modeling of MOF/polymer MMMs is the full atomistic simulation where MOF and polymer were simulated together. Jiang's group [101] simulated the polymer phase at the atomistic level similar to the MOF phase and studied ZIF-7/polybenzimidazole (PBI) MMMs where ZIF-7 was modeled using a newly developed force field and PBI was mimicked by the polymer-consistent force field. Predicted density and glass transition temperature of PBI were reported to be in a reasonably good agreement with experimental measurements. Addition of ZIF-7 improved the bulk modulus of PBI/ZIF-7 membranes indicating that it has stronger mechanical strength than PBI. Authors also discussed that although there are differences between the simulated and experimental results of pristine PBI and ZIF-7. This fully atomistic approach is of course computationally demanding compared to the first approach since a polymer is represented at the atomic scale in addition to the MOF using specific force fields.

As the numbers of MOFs and computational powers have continuously increased, large-scale computational screening of MOFs has become an important field. Altintas and Keskin [100] used a computational screening approach having increasing complexity at each step to study 3794 different MOFs for CO_2/CH_4 separation. Gas permeabilities of MOFs were computed combining the Henry's constant obtained from GCMC simulations and diffusivities obtained from MD simulations, which were all performed at infinite dilution to save computational time. CO_2 and CH_4 permeability data of the top eight MOFs obtained from this initial computational screening were then combined with the experimental gas permeability data of eight polymers and permeability of 64 different MOF-based MMMs were predicted using the Maxwell permeation model. The gas permeabilities of MOF fillers (P_{MOF}) were found to be very high compared to those of polymers (P_P). When $P_{MOF} >> P_P$, the Maxwell model reduces to $P_{MMM} = P_P \times 1.75$, where P_{MMM} represents the permeability of the MMM at a filler volume fraction of 0.2. As a result of this, the type of MOF filler was found to have an insignificant effect on the gas permeability of many MMMs. On the other hand, several MOF fillers were identified to improve the polymers' performances, both the CO_2 permeability and selectivity, and even to carry polymers over the upper bound if the polymer is close to the upper bound.

Wilmer's group [102] studied a very large numbers of MOFs as fillers in MMMs for CO_2/N_2 separation. They combined GCMC and MD simulations to compute CO_2 permeabilities and CO_2/N_2 selectivities of 112888 real and hypothetical (computer-generated) MOF structures at infinite dilution. This data was then combined with the experimentally measured CO_2 and N_2 permeabilities of nine polymers and gas permeabilities of MOF/polymer MMMs were predicted using the Maxwell model. Results showed that there are many MOFs for which using them as fillers in highly permeable polymers can lead to the MMMs that can exceed the Robeson's upper bound for CO_2/N_2 separation. Authors also reported that MMMs having polymers with low CO_2 permeability such as Matrimid are unlikely to exceed the upper bound when the MOFs were added into the polymer. One important outcome of this work was that a connection between molecular simulations and the cost of carbon capture was developed which was predicted as a function of membrane's CO_2 permeability and CO_2/N_2 selectivity. MOFs with CO_2 permeability or CO_2/N_2 selectivity lower than that of the neat polymer were estimated to produce MMMs having high cost of carbon capture. MOFs leading to membranes predicted to have the best cost of carbon capture were found to have 100 times higher CO_2 permeability than that of polymer and roughly 1000 times larger CO_2/N_2 selectivity than the polymer. To sum up, high-throughput screening of MOFs as filler will be very useful to direct the experimental researchers to the best MOF filler candidates for the fabrication of the MOF/polymer MMMs. The next question here is the compatibility between the MOF filler and the polymer.

7. Understanding the MOF/Polymer Compatibility: The Role of Computational Tools

The compatibility between the filler and polymer is highly important for the preparation of high performance MMMs. The review of current literature shows that MOF-based MMMs offer a great promise in high-performance gas separations. However, a major challenge in this field is the appropriate selection of the polymer and MOF that will lead to a good compatibility. It has been

discussed that the MOF/polymer compatibility in the MMMs has been reported to be poor and only low MOF filler loadings were achieved before the membrane selectivity is negatively affected [92]. Zhu et al. [80] reviewed the existing solutions and strategies utilized to improve MOF/polymer compatibility. The MOF/polymer interface dictates feasibility and stability of MOF/polymer MMMs, therefore fundamental understanding of this interface is critical.

Atomistic simulations can provide insights into the interactions at the MOF/polymer interface but the number of computational studies on this topic is very limited. Maurin's group [103] studied ZIF-8/PIM-1 MMM by introducing a computational method combining the density functional theory (DFT) calculations and MD simulations to model MOF/polymer interfaces. MOF surfaces were constructed and geometry-optimized using the DFT calculations and polymer was constructed at the atomic level. Force field-based MD simulations were used to construct reliable models for the MOF/polymer interface. Figure 8 represents the methodology they developed for the generation of the MOF/polymer interface. The details of MD steps at different ensembles such as temperature, pressure and length of the simulations used in the process of the MOF/polymer interface generation can be found in the corresponding work. Results showed that there is an interaction between the −CN groups of PIM-1 and NH terminal functions of the organic linker at the ZIF-8 surface. As a result, polymer caused to interfacial micro-voids at the vicinity of the MOF surface. The polydispersity of the polymer and the flexibility of the MOF surface were found to only slightly affect the properties of the interface. This methodology can be used to examine the potential affinity between different MOF surfaces and polymers, but it is important to note that the force field representing the correct description of the MMM is required in order to successfully transfer this methodology to other MOF/polymer MMMs.

The same group [104] also examined ZIF-8/PIM-1 membranes using molecular simulations and experiments. Their results showed that the microstructure of MMMs is based on many features including the molecular structure and rigidity of polymer and MOF/polymer interactions. It was found that using MOFs having an organic linker that is structurally similar to polymer's monomer can be a potential strategy to improve the interfacial properties of MMMs. Considering the fact that ZIF-8 is one of the most widely used MOF fillers in the MMM applications, examining the compatibility of ZIF-8 with different types of polymers having various rigidity will be a future direction in this field.

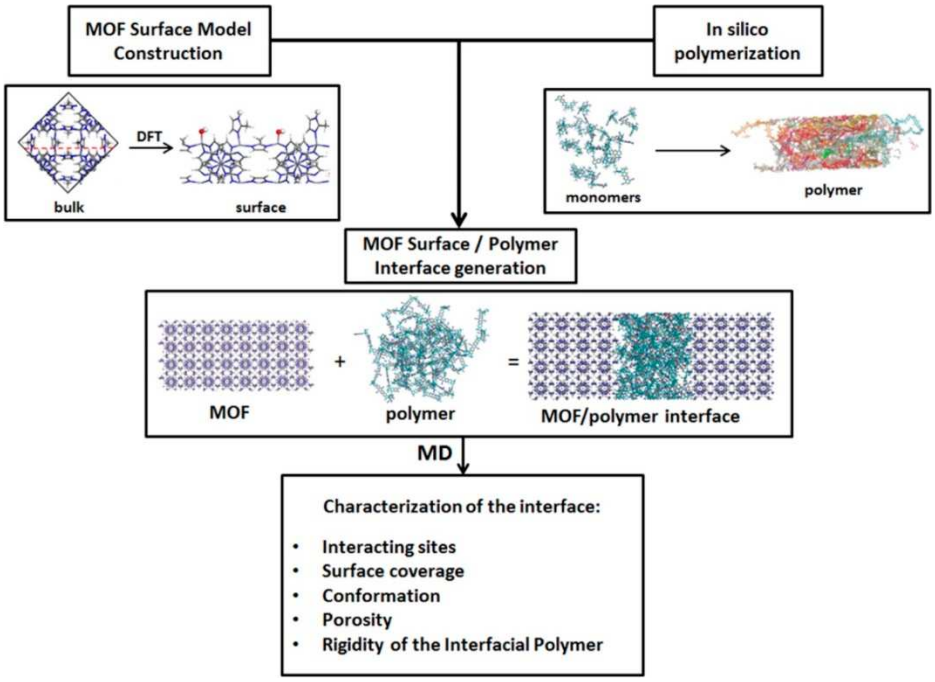


Figure 8. Methodology developed for the generation of the MOF/polymer interface and its characterization. Reprinted from Ref. [103] with permission from American Chemical Society.

A recent computational study focused on systematically investigating the structure of UiO-66/polymer interfaces combining force field and quantum-based molecular simulations [105]. Similar to the previous works, the MOF surface and polymer were constructed separately and then further combined to build different interfaces. Three different polymers, PIM-1, polystyrene (PS) and polyethylene glycol (PEG) were examined and results demonstrated that polymer rigidity negatively affect the MOF/polymer compatibility. UiO-66/PEG composite was predicted to show an excellent compatibility and strong MOF/polymer interactions with the penetration of a polymer in the first layers of the UiO-66 surface as confirmed by the experiments. Results of computational and experimental studies showed that polymers that have Young's modulus values <1 GPa are highly compatible systems. Similar types of computational studies examining a particular type of MOF and several different polymers with different physical and chemical properties (i.e., different chain lengths and rigidities) will be very useful in establishing the guidelines to identify MOF/polymer pairs that will lead to stable, highly compatible MMMs. Furthermore, studying MOFs having different levels of flexibilities, pore sizes and chemical functionalities, will provide a deeper understanding the impacts of the type of the filler on the MOF/polymer interface. Future computational studies in this field will direct the experimentalists to choose the best MOF/polymer pairs with high compatibility to guarantee the feasibility of the MMMs for gas separation applications.

The absence of organic linkers or metal centers can cause point defects in MOF structures and these defects can be even engineered to improve the performance of MOFs in different applications [106,107]. Semino et al. [108] coupled MD simulations with quantum calculations to understand the MOF/polymer compatibility in the presence of defects at the MOF surface. They studied defect-containing ZIF-8/PIM composites and compared their results with those of the defect-free interfaces. Their computational results demonstrated that MOF/polymer interactions vary in the presence of defects, however, the morphology of the interfacial micro-voids was the same from a microscopic point of view. This finding suggests that properties such as geometry and flexibility mainly dictate the structure of the MOF/polymer interface, while the chemical interactions only have a small impact.

A recent approach in modeling MOF/polymer compatibility is combining atomistic and coarse grained (CG) force field-based MD simulations. The main motivation behind using a CG model is that this approach groups several atoms into a single interacting site that is called a bead and reduces the total number of particles. As a result, force field-based MD simulations become much less computationally expensive. Maurin's group [109] introduced a multi-scale study combining micro- and mesoscopic resolution, by coupling atomistic and CG simulations to examine HKUST-1/poly(vinyl alcohol) MMM. The CG model reproduced the relevant features of the MOF/polymer interface in a very good agreement with the atomistic model and penetration of the polymer into the pores of the MOF was shown. In contrast to the previously discussed ZIF-8/PIM interfaces, there was no interfacial void, indicating the very good MOF/polymer affinity. Extension of the CG method to explore MOF nanoparticles incorporated into the polymers will be important to unlock the interfacial phenomena in MMMs.

8. The Role of Computational Studies in Analyzing the Barriers That Must Be Overcome to Advance MOF-Based Membranes Beyond Fundamental Characterizations

(i) Combination of experiments and molecular simulations: We so far attempted to provide a brief review of computational studies to understand the gas separation performance of MOF/polymer MMMs and the compatibility issues between the MOF filler and polymer in the composite membrane. As we discussed in the beginning, gas transport through a composite membrane is a complex problem and combination of fundamental experimental and computational studies is always desired to unlock the mass transfer of gases through MMMs. A great example is the recent work of Karger's group [110] where microimaging by infrared (IR) microscopy was combined with molecular simulations to understand the evolution of CO_2 concentration in the ZIF-8/6FDA-DAM MMM. The time-resolved IR images showed that CO_2 molecules propagate from the MOF filler to the surrounding polymer

in addition to the observation of the enhancement of CO_2 concentration at the interface between the polymer and the filler at equilibrium. Molecular simulations demonstrated that CO_2 molecules generally tend to accumulate in the micro-voids at the MOF/polymer interface. Coronas's group [111] also combined experiments and molecular simulations to examine a 6FDA-DAM-based MMM with a different MOF filler, UiO-66, and reported enhanced gas separation performance of the MMM. Zhao et al. [112] incorporated MOF nanosheets, NUS-8, into PIM-1 to prepare MMMs. Molecular simulations combining the DFT calculations and force field-based MD simulations supported the experimental findings that there is a good compatibility between PIM-1 and NUS-8 because of the filler/polymer interactions. As these works show combination of experiments and computational studies will be very useful for the systematic investigation of design parameters of MOF/polymer MMMs such as the type of MOF structure and polymer, loading of the MOF filler. Fundamental understanding of the MMM structure, especially understanding the interactions between MOFs and polymers and their impacts on the overall gas separation performance of MMMs can provide guidelines for the future design and development of new MOF/polymer MMMs.

(ii) High-throughput molecular simulations of MOF fillers: Another important point to discuss is that as we reviewed above, high-throughput computational screening of MOF fillers to be used in MOF/polymer MMMs is a quickly developing field. These studies generally computed gas transport properties of MOFs at infinite dilution where the interactions between adsorbed gas molecules are neglected to save computational time and then this data was used to predict the gas transport in MOF/polymer MMMs. However, MMMs operate at a predefined pressure and in fact pressure is one of the parameters that can be altered to achieve the optimal gas separation performance of the MMMs. Furthermore, this type of MMM calculations used molecular simulations only for MOFs and utilized the available experimental data of polymers. Since the MOF and polymer were not simulated together at the atomistic level, interactions between the polymer and MOF particles were not considered in this type of studies. Size, orientation and/or distribution of the MOF fillers in polymers were not taken into account and theoretical permeation models were used to estimate the gas permeability of the MMM using the simulated permeability data of MOFs and experimental permeability data of polymers. In practice, particle size of the fillers may lead to different concentrations of the non-selective pathways, which overall affect the separation performance of the MMM. In summary, high-throughput computational screening studies are generally performed to identify a small number of promising MOF fillers that offer the best combination of gas permeability and selectivity. The issues that we highlighted above such as the compatibility between MOF and polymer, the stability of the resulting MOF/polymer MMM, change in the gas separation performance of the MMM depending on the operating pressure, etc. are more likely to be tested and addressed by further experimental studies. As we noted above, extension of this type of high-throughput screening approaches to ILs will be also very useful to study IL/MOF/polymer MMMs, which are currently experimentally tested.

(iii) Unlocking the potential of MOFs for different gas separations: Most of the current studies have focused on experimental testing and computational modeling of MOF-based MMMs for CO_2 separation due to the importance of flue gas separation and natural gas purification. A membrane that offers low performance for a particular gas separation can be very promising for another gas separation process. Further studies on separation of different gas mixtures such as air separation, hydrocarbon separation would be very useful. For example, a recent experimental work [113] reported that MOF-based polyimide MMMs can exhibit enhanced ethylene/ethane selectivity with greater ethylene permeability and improved membrane stability, hinting the potential of MOF/polymer membranes for hydrocarbon separations. Further computational studies in this field are required to understand the potential of MMMs in various types of gas separations.

Finally, it is important to discuss the limitations of molecular simulations used to predict gas separation performances of MOF/polymer MMMs. Molecular simulations generally assume perfect, defect-free, rigid MOF structures but defects and inter-crystalline paths may exist in synthesized MOFs. Some MOFs are known to be flexible and flexibility may significantly affect the transport of gas

molecules through the pores of MOFs. Molecular simulations utilize generic force fields to compute gas adsorption and diffusion in MOFs. However, these force fields may not be accurately representing the interaction between the gas molecules and MOF atoms in some special cases such as the presence of open metal sites in MOFs. Besides these, MOFs can have chemical/thermal stability issues but molecular simulations generally do not provide insights into the stability of MOFs. Therefore, the best MOF fillers identified from high-throughput molecular simulation studies should be examined by further experiments in detail to resolve stability and compatibility issues.

9. Concluding Remarks and Future Directions

Research over the last two decades has shown that MMMs can surpass the upper bound between permeability and selectivity for gas separation applications. The design space for MMMs is very large and computational tools can guide the experimental efforts in the design of new materials by characterizing both filler and polymer in silico prior to actual synthesis and by matching the filler and polymer to manufacture the membrane with the desired transport properties. Theories of trade-off behavior suggest that in order to surpass the upper bound, both sorption and diffusion selectivities should be improved. Using high-throughput computational tools, it is possible to determine the specific adsorption sites for gas molecules within the structure that are responsible for highly selective adsorption. In addition, the effects of various functionalization or the specific treatments of the polymers on the sorption selectivity and the choice of monomers for the polymer design can be rapidly screened with molecular simulations. Although significant progress has been made on the molecular simulations for fillers, polymers and their combinations in the MMMs, there are still challenges for the computations. First of all, the state-of-the-art force fields should be selected and validated to obtain reliable information from the simulations. Second, in silico synthesis of the hypothetical new materials should not require any experimental input data for the computations. In other words, new algorithms should be developed to construct polymers without requiring experimental data inputs. Third, swelling, plasticization and aging of the polymer that are all known to affect both the permeability and selectivity should be taken into account in the simulations. The current literature indicates that to advance the field, future studies should focus on developing computational tools that can provide structure-property relationship under industrially relevant conditions such as temperature, pressure, as well as processing conditions. In addition, computational algorithms that can be used to investigate the effects of concentration, structure, shape and functionality of the fillers on the gas transport properties are needed. In conclusion, we can claim that combining cutting-edge experiments and innovative simulations can lead to the development of membrane materials that can significantly exceed the upper-bound for various gas separation applications.

Funding: This research received no external funding.

Conflicts of Interest: The authors declare no conflict of interest.

References

1. Robeson, L.J. Correlation of Separation Factor Versus Permeability for Polymeric Membranes. *J. Membr. Sci.* **1991**, *62*, 165–185. [CrossRef]
2. Freeman, B.D. Basis of permeability/selectivity tradeoff relations in polymeric gas separation membranes. *Macromolecules* **1999**, *32*, 375–380. [CrossRef]
3. Burns, R.L.; Koros, W.J. Defining the challenges for C_3H_6/C_3H_8 separation using polymeric membranes. *J. Membr. Sci.* **2003**, *211*, 299–309. [CrossRef]
4. Rungta, M.; Zhang, C.; Koros, W.J.; Xu, L.R. Membrane-based ethylene/ethane separation: The upper bound and beyond. *AIChE J.* **2013**, *59*, 3475–3489. [CrossRef]
5. Rowe, B.W.; Robeson, L.M.; Freeman, B.D.; Paul, D.R. Influence of temperature on the upper bound: Theoretical considerations and comparison with experimental results. *J. Membr. Sci.* **2010**, *360*, 58–69. [CrossRef]

6. Alentiev, A.Y.; Yampolskii, Y.P. Correlation of gas permeability and diffusivity with selectivity: Orientations of the clouds of the data points and the effects of temperature. *Ind. Eng. Chem. Res.* **2013**, *52*, 8864–8874. [CrossRef]
7. Alentiev, A.Y.; Yampolskii, Y.P. Free volume model and tradeoff relations of gas permeability and selectivity in glassy polymers. *J. Membr. Sci.* **2000**, *165*, 201–216. [CrossRef]
8. Alentiev, A.Y.; Yampolskii, Y.P. Meares equation and the role of cohesion energy density in diffusion in polymers. *J. Membr. Sci.* **2002**, *206*, 291–306. [CrossRef]
9. Lou, Y.C.; Hao, P.J.; Lipscomb, G. NELF predictions of a solubility–solubility selectivity upper bound. *J. Membr. Sci.* **2014**, *455*, 247–253. [CrossRef]
10. Lin, H.; Yavari, M. Upper bound of polymeric membranes for mixed-gas CO_2/CH_4 separations. *J. Membr. Sci.* **2015**, *475*, 101–109. [CrossRef]
11. Budd, P.M.; McKeown, N.B. Highly permeable polymers for gas separation membranes. *Polym. Chem.* **2010**, *1*, 63–68. [CrossRef]
12. Wiegand, J.R.; Smith, Z.P.; Liu, Q.; Patterson, C.T.; Freeman, B.D.; Guo, R.L. Synthesis and characterization of triptycene-based polyimides with tunable high fractional free volume for gas separation membranes. *J. Mater. Chem. A* **2014**, *2*, 13309–13320. [CrossRef]
13. Singh, A.; Koros, W.J. Significance of entropic selectivity for advanced gas sep-aration membranes. *Ind. Eng. Chem. Res.* **1996**, *35*, 1231–1234. [CrossRef]
14. Goh, P.S.; Ismail, A.F.; Sanip, S.M.; Ng, B.C.; Aziz, M. Recent advances of inorganic fillers in mixed matrix membrane for gas separation. *Sep. Purif. Technol.* **2011**, *81*, 243–264. [CrossRef]
15. Park, H.B.; Kamcev, J.; Robeson, L.M.; Elimelech, M.; Freeman, B.D. Maximizing the right stuff: The trade-off between membrane permeability and selectivity. *Science* **2017**, *356*, eaab0530. [CrossRef] [PubMed]
16. Sen, D.; Kalipcilar, H.; Yilmaz, L. Development of polycarbonate based zeolite 4A filled mixed matrix gas separation membranes. *J. Membr. Sci.* **2007**, *303*, 194–203. [CrossRef]
17. Sen, D.; Kalipcilar, H.; Yilmaz, L. Development of zeolite filled polycarbonate mixed matrix gas separation membranes. *Desalination* **2006**, *200*, 222–224. [CrossRef]
18. Tantekin-Ersolmaz, S.B.; Atalay-Oral, C.; Tather, M.; Erdem-Senatalar, A.; Schoeman, B.; Sterte, J. Effect of zeolite particle size on the performance of polymer-zeolite mixed matrix membranes. *J. Membr. Sci.* **2000**, *175*, 285–288. [CrossRef]
19. Pechar, T.W.; Kim, S.; Vaughan, B.; Marand, E.; Tsapatsis, M.; Jeong, H.K.; Cornelius, C.J. Fabrication and characterization of polyimide-zeolite L mixed matrix membranes for gas separations. *J. Membr. Sci.* **2006**, *277*, 195–202. [CrossRef]
20. Husain, S.; Koros, W.J. Mixed matrix hollow fiber membranes made with modified HSSZ-13 zeolite in polyetherimide polymer matrix for gas separation. *J. Membr. Sci.* **2007**, *288*, 195–207. [CrossRef]
21. Gorgojo, P.; Zornoza, B.; Uriel, S.; Telelz, C.; Coronas, J. Mixed Matrix Membranes from Nanostructured Materials for Gas Separation. *Stud. Surf. Sci. Catal.* **2008**, *174*, 653–656.
22. Pechar, T.W.; Kim, S.; Vaughan, B.; Marand, E.; Baranauskas, V.; Riffle, J.; Jeong, H.K.; Tsapatsis, M. Preparation and characterization of a poly(imide siloxane) and zeolite L mixed matrix membrane. *J. Membr. Sci.* **2006**, *277*, 210–218. [CrossRef]
23. Zeng, C.; Zhang, L.; Cheng, X.; Wang, H.; Xu, N. Preparation and gas permeation of nano-sized zeolite NaA-filled carbon membranes. *Sep. Purif. Technol.* **2008**, *63*, 628–633. [CrossRef]
24. Li, Y.; Chung, T.-S.; Cao, C.; Kulprathipanja, S. The effects of polymer chain rigidification, zeolite pore size and pore blockage on polyethersulfone (PES)-zeolite A mixed matrix membranes. *J. Membr. Sci.* **2005**, *260*, 45–55. [CrossRef]
25. Clarizia, G.; Algieri, C.; Regina, A.; Drioli, E. Zeolite-based composite PEEK-WC membranes: Gas transport and surface properties. *Microporous Mesoporous Mater.* **2008**, *115*, 67–74. [CrossRef]
26. Vu, D.Q.; Koros, W.J.; Miller, S.J. Mixed matrix membranes using carbon molecular sieves—I. Preparation and experimental results. *J. Membr. Sci.* **2003**, *211*, 311–334. [CrossRef]
27. Moore, T.T.; Mahajan, R.; Vu, D.Q.; Koros, W.J. Hybrid membrane materials comprising organic polymers with rigid dispersed phases. *AIChE J.* **2004**, *50*, 311–321. [CrossRef]
28. Vu, D.Q.; Koros, W.J.; Miller, S.J. Effect of condensable impurity in CO2/CH4 gas feeds on performance of mixed matrix membranes using carbon molecular sieves. *J. Membr. Sci.* **2003**, *221*, 233–239. [CrossRef]

29. Das, M.; Perry, J.D.; Koros, W.J. Gas-Transport-Property Performance of Hybrid Carbon Molecular Sieve-Polymer Materials. *Ind. Eng. Chem. Res.* **2010**, *49*, 9310–9321. [CrossRef]
30. Vu, D.Q.; Koros, W.J.; Miller, S.J. Mixed matrix membranes using carbon molecular sieves—II. Modeling permeation behavior. *J. Membr. Sci.* **2003**, *211*, 335–348. [CrossRef]
31. Shimekit, B.; Muktar, H.; Maitra, S. Comparison of Predictive Models for Relative Permeability of CO_2 in Matrimid-Carbon Molecular Sieve Mixed Matrix Membrane. *J. Appl. Sci.* **2010**, *10*, 1204–1211. [CrossRef]
32. Kusakabe, K.; Ichiki, K.; Hayashi, J.-I.; Maeda, H.; Morroka, S. Preparation and characterization of silica-polyimide composite membranes coated on porous tubes for CO_2 separation. *J. Membr. Sci.* **1996**, *115*, 65–75. [CrossRef]
33. Moadded, M.; Koros, W.J. Effects of colloidal silica incorporation on oxygen nitrogen separation properties of ceramic-supported 6FDA-IPDA thin films. *J. Membr. Sci.* **1996**, *111*, 283–290. [CrossRef]
34. Zornoza, B.; Tellex, C.; Coronas, J. Mixed matrix membranes comprising glassy polymers and dispersed mesoporous silica spheres for gas separation. *J. Membr. Sci.* **2011**, *368*, 100–109. [CrossRef]
35. Merkel, T.C.; He, Z.; Pinnau, I. Effect of nanoparticles on gas sorption and transport in poly(1-trimethylsilyl-1-propyne). *Macromolecules* **2003**, *36*, 6844–6855. [CrossRef]
36. Merkel, T.C.; Freeman, B.D.; Spontak, R.J.; He, Z.; Pinnau, I.; Meakin, P.; Hill, A.J. Sorption, transport, and structural evidence for enhanced free volume in poly(4-methyl-2-pentyne)/fumed silica nanocomposite membranes. *Chem. Mater.* **2003**, *15*, 109–123. [CrossRef]
37. Hosseini, S.S.; Li, Y.; Chung, T.-S.; Liu, Y. Enhanced gas separation performance of nanocomposite membranes using MgO nanoparticles. *J. Membr. Sci.* **2007**, *302*, 207–217. [CrossRef]
38. Matteucci, S.; Raharjo, R.D.; Kusuma, V.A.; Swinnea, S.; Freeman, B.D. Gas Permeability, Solubility, and Diffusion Coefficients in 1,2-Polybutadiene Containing Magnesium Oxide. *Macromolecules* **2008**, *41*, 2144–2156. [CrossRef]
39. Chen, H.; Sholl, D.S. Predictions of selectivity and flux for CH_4/H-2 separations using single walled carbon nanotubes as membranes. *J. Membr. Sci.* **2006**, *269*, 152–160. [CrossRef]
40. Skoulidas, A.I.; Sholl, D.S.; Johnson, J.K. Adsorption and diffusion of carbon dioxide and nitrogen through single-walled carbon nanotube membranes. *J. Chem. Phys.* **2004**, *124*, 054708. [CrossRef]
41. Cong, H.; Zhang, J.; Radosx, M.; Shen, Y. Carbon nanotube composite membranes of brominated poly(2,6-diphenyl-1,4-phenylene oxide) for gas separation. *J. Membr. Sci.* **2007**, *294*, 178–185. [CrossRef]
42. Ge, L.; Zhu, Z.; Rudolph, V. Enhanced gas permeability by fabricating functionalized multi-walled carbon nanotubes and polyethersulfone nanocomposite membrane. *Sep. Purif. Technol.* **2011**, *78*, 76–82. [CrossRef]
43. Ge, L.; Zhu, Z.; Li, F.; Liu, S.; Wang, L.; Tang, X.; Rudolph, V. Investigation of Gas Permeability in Carbon Nanotube (CNT)-Polymer Matrix Membranes via Modifying CNTs with Functional Groups/Metals and Controlling Modification Location. *J. Phys. Chem. C* **2011**, *115*, 6661–6670. [CrossRef]
44. Goh, P.S.; Ng, B.C.; Ismail, A.F.; Sanip, S.M.; Aziz, M.; Kassim, M.A. Effect of Dispersed Multi-Walled Carbon Nanotubes on Mixed Matrix Membrane for O_2/N_2 Separation. *Sep. Sci. Technol.* **2011**, *46*, 1250–1261. [CrossRef]
45. Aroon, M.A.; Ismail, A.F.; Montazer-Rahmati, M.M.; Matsuura, T. Effect of chitosan as a functionalization agent on the performance and separation properties of polyimide/multi-walled carbon nanotubes mixed matrix flat sheet membranes. *J. Membr. Sci.* **2010**, *364*, 309–317. [CrossRef]
46. Weng, T.-H.; Tseng, H.-H.; Wey, M.-Y. Preparation and characterization of multi-walled carbon nanotube/PBNPI nanocomposite membrane for H-2/CH_4 separation. *Int. J. Hydrog. Energy* **2009**, *34*, 8707–8715. [CrossRef]
47. Kim, S.; Chen, L.; Johnson, J.K.; Marand, E. Polysulfone and functionalized carbon nanotube mixed matrix membranes for gas separation: Theory and experiment. *J. Membr. Sci.* **2007**, *294*, 147–158. [CrossRef]
48. Kim, S.; Pechar, T.W.; Marand, E. Poly(imide siloxane) and carbon nanotube mixed matrix membranes for gas separation. *Desalination* **2006**, *192*, 330–339. [CrossRef]
49. Leszczynska, A.; Njuguna, J.; Pielichowski, K.; Banerjee, J.R. Polymer/montmorillonite nanocomposites with improved thermal properties. Part II. Thermal stability of montmorillonite nanocomposites based on different polymeric matrixes. *Thermochim. Acta* **2007**, *454*, 1–22. [CrossRef]
50. Defontaine, G.; Barichard, A.; Letaief, S.; Feng, C.; Matsuura, T.; Detellier, C. Nanoporous polymer—Clay hybrid membranes for gas separation. *Colloid. Interface Sci.* **2010**, *343*, 622–627. [CrossRef]

51. Wu, Y.; Jia, P.; Xu, L.L.; Chen, Z.Y.; Xiao, L.H.; Sun, J.H.; Zhang, J.; Huang, Y.; Bielawski, C.W.; Geng, J.X. Tuning the surface properties of graphene oxide by surface-initiated polymerization of epoxides: An efficient method for enhancing gas separation. *ACS Appl. Mater. Interfaces* **2017**, *9*, 4998–5005. [CrossRef] [PubMed]
52. Karunakaran, M.; Shevate, R.; Kumar, M.; Peinemann, K.V. CO_2-selective PEO-PBT (PolyActive)/graphene oxide composite membranes. *Chem. Commun.* **2015**, *51*, 14187–14190. [CrossRef] [PubMed]
53. Kim, S.; Hou, J.; Wang, Y.Q.; Ou, R.W.; Simon, G.P.; Seong, J.G.; Lee, Y.M.; Wang, H.T. Highly permeable thermally rearranged polymer composite membranes with a graphene oxide scaffold for gas separation. *J. Mater. Chem. A.* **2018**, *6*, 7668–7674. [CrossRef]
54. Dong, G.; Hou, J.; Wang, J.; Zhang, Y.; Chen, V.; Liu, J. Enhanced CO_2/N_2 separation by porous reduced graphene oxide/Pebax mixed matrix membranes. *J. Membr. Sci.* **2016**, *520*, 860–868. [CrossRef]
55. Berean, K.J.; Ou, J.Z.; Nour, M.; Field, M.R.; Alsaif, M.M.Y.A.; Wang, Y.; Ramanathan, R.; Bansal, V.; Kentish, S.; Doherty, C.M.; et al. Enhanced gas permeation through graphene nanocomposites. *J. Phys. Chem. C* **2015**, *119*, 13700–13712. [CrossRef]
56. Zimmerman, C.M.; Singh, A.; Koros, W.J. Tailoring mixed matrix composite membranes for gas separations. *J. Membr. Sci.* **1997**, *137*, 145–154. [CrossRef]
57. Te Hennepe, H.J.C.; Smolders, C.A.; Bargeman, D.; Mulder, M.H.V. Exclusion and Tortuosity Effects for Alcohol/Water Separation by Zeolite-Filled PDMS Membranes. *Sep. Sci. Technol.* **1991**, *26*, 585–596. [CrossRef]
58. Cussler, E.L. Membranes containing selective flakes. *J. Membr. Sci.* **1990**, *52*, 275–288. [CrossRef]
59. Ebneyamini, A.; Azimi, H.; Tezel, F.H.; Thibault, J. Mixed matrix membranes applications: Development of a resistance-based model. *J. Membr. Sci.* **2017**, *543*, 351–360. [CrossRef]
60. Kang, D.-Y.; Jones, C.W.; Nair, S. Modeling molecular transport in composite membranes with tubular fillers. *J. Membr. Sci.* **2011**, *381*, 50–63. [CrossRef]
61. Cosenza, P.; Ghorbani, A.; Camerlynck, C.; Rejiba, F.; Guerin, R.; Tabbagh, A. Effective medium theories for modelling the relationships between electromagnetic properties and hydrological variables in geomaterials: A review. *Near Surf. Geophys.* **2009**, *7*, 563–578. [CrossRef]
62. Pal, R. Newmodels for thermal conductivity of particulate composites. *J. Reinf. Plast. Compos.* **2007**, *26*, 643–651. [CrossRef]
63. Chiew, Y.C.; Glandt, E.D. The effect of structure on the conductivity of a dispersion. *J. Colloid Interface Sci.* **1983**, *94*, 90–104. [CrossRef]
64. Jeffrey, D.J. Conduction through a Random Suspension of Spheres. *Proc. R. Soc. Lond. A Math. Phys. Eng. Sci.* **1973**, *335*, 355–367. [CrossRef]
65. Landauer, R.; Garland, J.C.; Tanner, D.B. Electrical Conductivity in inhomogeneous media. *AIP Conf. Proc.* **1978**, *40*, 2–45.
66. Higuchi, W.I. A New Relationship for the Dielectric Properties of Two Phase Mixtures. *J. Phys. Chem.* **1958**, *62*, 649–653. [CrossRef]
67. Te Hennepe, H.J.C.; Boswerger, W.B.F.; Bargeman, D.; Mulder, M.H.V.; Smolders, C.A. Zeolite-filled silicone rubber membranes experimental determination of concentration profiles. *J. Membr. Sci.* **1994**, *89*, 185–196. [CrossRef]
68. Falla, W.R.; Mulski, M.; Cussler, E.L. Estimating diffusion through flake-filled membranes. *J. Membr. Sci.* **1996**, *119*, 129–138. [CrossRef]
69. Maxwell, J.C. *A Treatise on Electricity and Magnetism*; Clarendon Press: Oxford, UK, 1873.
70. Bouma, R.H.B.; Checchetti, A.; Chidichimo, G.; Drioli, E. Permeation through a heterogeneous membrane: The effect of the dispersed phase. *J. Membr. Sci.* **1997**, *128*, 141–149. [CrossRef]
71. Lewis, T.B.; Nielsen, L.E. Dynamic mechanical properties of particulate-filled Composites. *J. Appl. Polym. Sci.* **1970**, *14*, 1449–1471. [CrossRef]
72. Felske, J.D. Effective thermal conductivity of composite spheres in a continuous medium with contact resistance. *Int. J. Heat Mass Transf.* **2004**, *47*, 3453–3461. [CrossRef]
73. Shimekit, B.; Mukhtar, H.; Murugesan, T. Prediction of the relative permeability of gases in mixed matrix membranes. *J. Membr. Sci.* **2011**, *373*, 152–159. [CrossRef]
74. Mahajan, R.; Koros, W.J. Mixed matrix membrane materials with glassy polymers. Part 1. *Polym. Eng. Sci.* **2002**, *42*, 1420–1431. [CrossRef]

75. Fang, M.; Wu, C.; Yang, Z.; Wang, T.; Xia, Y.; Li, J. ZIF-8/PDMS mixed matrix membranes for propane/nitrogen mixtureseparation: Experimental result and permeation model validation. *J. Membr. Sci.* **2015**, *474*, 103–113. [CrossRef]
76. Shariati, A.; Omidkhah, M.; Pedram, M.Z. New permeation models for nanocomposite polymeric membranes filled with nonporous particles. *Chem. Eng. Res. Des.* **2012**, *90*, 563–575. [CrossRef]
77. Aroon, M.A.; Ismail, A.F.; Matsuura, T.; Montazer-Rahmati, M.M. Performance studies of mixed matrix membranes for gas separation: A review. *Sep. Purif. Technol.* **2010**, *75*, 229–242. [CrossRef]
78. Monsalve-Bravo, G.M.; Bhatia, S.K. Modeling Permeation through Mixed-Matrix Membranes: A Review. *Processes* **2018**, *6*, 172. [CrossRef]
79. Monsalve-Bravo, G.M.; Bhatia, S.K. Concentration-dependent transport in finite sized composites: Modified effective medium theory. *J. Membr. Sci.* **2018**, *550*, 110–125. [CrossRef]
80. Lin, R.; Hernandez, B.V.; Ge, L.; Zhu, Z. Metal organic framework based mixed matrix membranes: An overview on filler/polymer interfaces. *J. Mater. Chem. A* **2018**, *6*, 293–312. [CrossRef]
81. Dai, L.; Yu, S.; Shan, Y.; He, M. Novel room temperature inorganic ionic liquids. *Eur. J. Inorg. Chem.* **2004**, *2004*, 237–241. [CrossRef]
82. Marsh, K.; Boxall, J.; Lichtenthaler, R. Room temperature ionic liquids and their mixtures—A review. *Fluid Phase Equilib.* **2004**, *219*, 93–98. [CrossRef]
83. Hao, L.; Liao, K.-S.; Chung, T.-S. Photo-oxidative PIM-1 based mixed matrix membranes with superior gas separation performance. *J. Mater. Chem. A* **2015**, *3*, 17273–17281. [CrossRef]
84. Li, H.; Tuo, L.; Yang, K.; Jeong, H.-K.; Dai, Y.; He, G.; Zhao, W. Simultaneous enhancement of mechanical properties and CO_2 selectivity of ZIF-8 mixed matrix membranes: Interfacial toughening effect of ionic liquid. *J. Membr. Sci.* **2016**, *511*, 130–142. [CrossRef]
85. Ban, Y.; Li, Z.; Li, Y.; Peng, Y.; Jin, H.; Jiao, W.; Guo, A.; Wang, P.; Yang, Q.; Zhong, C. Confinement of ionic liquids in nanocages: Tailoring the molecular sieving properties of ZIF-8 for membrane-based CO_2 capture. *Angew. Chem. Int. Ed.* **2015**, *54*, 15483–15487. [CrossRef] [PubMed]
86. Lin, R.; Ge, L.; Diao, H.; Rudolph, V.; Zhu, Z. Ionic liquids as the MOFs/polymer interfacial binder for efficient membrane separation. *ACS Appl. Mater. Interfaces* **2016**, *8*, 32041–32049. [CrossRef] [PubMed]
87. Erucar, I.; Yilmaz, G.; Keskin, S. Recent advances in metal–organic framework-based mixed matrix membranes. *Chem. Asian J.* **2013**, *8*, 1692–1704. [CrossRef] [PubMed]
88. Erucar, I.; Keskin, S. Molecular modeling of MOF-based mixed matrix membranes. *Curr. Org. Chem.* **2014**, *18*, 2364–2380. [CrossRef]
89. Adatoz, E.; Avci, A.K.; Keskin, S. Opportunities and challenges of MOF-based membranes in gas separations. *Sep. Purif. Technol.* **2015**, *152*, 207–237. [CrossRef]
90. Erucar, I.; Keskin, S. Computational methods for MOF/polymer membranes. *Chem. Rec.* **2016**, *16*, 703–718. [CrossRef]
91. Pal, R. Permeation models for mixed matrix membranes. *J. Colloid Interface Sci.* **2008**, *317*, 191–198. [CrossRef]
92. Zornoza, B.; Tellez, C.; Coronas, J.; Gascon, J.; Kapteijn, F. Metal organic framework based mixed matrix membranes: An increasingly important field of research with a large application potential. *Microporous Mesoporous Mater.* **2013**, *166*, 67–78. [CrossRef]
93. Erucar, I.; Keskin, S. Separation of CO_2 mixtures using $Zn(bdc)(ted)_{0.5}$ membranes and composites: A molecular simulation study. *J. Phys. Chem. C* **2011**, *115*, 13637–13644. [CrossRef]
94. Erucar, I.; Keskin, S. Screening metal–organic framework-based mixed-matrix membranes for CO_2/CH_4 separations. *Ind. Eng. Chem. Res.* **2011**, *50*, 12606–12616. [CrossRef]
95. Erucar, I.; Keskin, S. Computational screening of metal organic frameworks for mixed matrix membrane applications. *J. Membr. Sci.* **2012**, *407*, 221–230. [CrossRef]
96. Yilmaz, G.; Keskin, S. Predicting the performance of zeolite imidazolate framework/polymer mixed matrix membranes for CO_2, CH_4, and H_2 separations using molecular simulations. *Ind. Eng. Chem. Res.* **2012**, *51*, 14218–14228. [CrossRef]
97. Yilmaz, G.; Keskin, S. Molecular modeling of MOF and ZIF-filled MMMs for CO_2/N_2 separations. *J. Membr. Sci.* **2014**, *454*, 407–417. [CrossRef]
98. Altintas, C.; Keskin, S. Molecular simulations of porous coordination network-based mixed matrix membranes for CO_2/N_2 separations. *Mol. Sim.* **2015**, *41*, 1396–1408. [CrossRef]

99. Sumer, Z.; Keskin, S. Computational screening of MOF-based mixed matrix membranes for CO_2/N_2 separations. *J. Nanomater.* **2016**, *2016*, 12. [CrossRef]
100. Altintas, C.; Keskin, S. Molecular simulations of MOF membranes and performance predictions of MOF/polymer mixed matrix membranes for CO_2/CH_4 Separations. *ACS Sustain. Chem. Eng.* **2018**, *7*, 2739–2750. [CrossRef]
101. Zhang, L.; Hu, Z.; Jiang, J. Metal–organic framework/polymer mixed-matrix membranes for H_2/CO_2 separation: A fully atomistic simulation study. *J. Phys. Chem. C* **2012**, *116*, 19268–19277. [CrossRef]
102. Budhathoki, S.; Ajayi, O.; Steckel, J.A.; Wilmer, C.E. High-throughput computational prediction of the cost of carbon capture using mixed matrix membranes. *Energy Environ. Sci.* **2019**, *12*, 1255–1264. [CrossRef]
103. Semino, R.; Ramsahye, N.A.; Ghoufi, A.; Maurin, G. Microscopic model of the metal–organic framework/polymer interface: A first step toward understanding the compatibility in mixed matrix membranes. *ACS Appl. Mater. Interfaces* **2016**, *8*, 809–819. [CrossRef] [PubMed]
104. Benzaqui, M.; Semino, R.; Menguy, N.; Carn, F.; Kundu, T.; Guigner, J.-M.; McKeown, N.B.; Msayib, K.J.; Carta, M.; Malpass-Evans, R.; et al. Toward an understanding of the microstructure and interfacial properties of PIMs/ZIF-8 mixed matrix membranes. *ACS Appl. Mater. Interfaces* **2016**, *8*, 27311–27321. [CrossRef] [PubMed]
105. Semino, R.; Moreton, J.C.; Ramsahye, N.A.; Cohen, S.M.; Maurin, G. Understanding the origins of metal–organic framework/polymer compatibility. *Chem. Sci.* **2018**, *9*, 315–324. [CrossRef] [PubMed]
106. St. Petkov, P.; Vayssilov, G.N.; Liu, J.; Shekhah, O.; Wang, Y.; Wöll, C.; Heine, T. Defects in MOFs: A thorough characterization. *ChemPhysChem* **2012**, *13*, 2025–2029. [CrossRef] [PubMed]
107. Yuan, L.; Tian, M.; Lan, J.; Cao, X.; Wang, X.; Chai, Z.; Gibson, J.K.; Shi, W. Defect engineering in metal–organic frameworks: A new strategy to develop applicable actinide sorbents. *Chem. Commun.* **2018**, *54*, 370–373. [CrossRef] [PubMed]
108. Semino, R.; Ramsahye, N.A.; Ghoufi, A.; Maurin, G. Role of MOF surface defects on the microscopic structure of MOF/polymer interfaces: A computational study of the ZIF-8/PIMs systems. *Microporous Mesoporous Mater.* **2017**, *254*, 184–191. [CrossRef]
109. Semino, R.; Dürholt, J.P.; Schmid, R.; Maurin, G. Multiscale modeling of the HKUST-1/Poly(vinyl alcohol) interface: From an atomistic to a coarse graining approach. *J. Phys. Chem. C* **2017**, *121*, 21491–21496. [CrossRef]
110. Hwang, S.; Semino, R.; Seoane, B.; Zahan, M.; Chmelik, C.; Valiullin, R.; Bertmer, M.; Haase, J.; Kapteijn, F.; Gascon, J.; et al. Revealing the transient concentration of CO_2 in a mixed-matrix membrane by IR microimaging and molecular modeling. *Angew. Chem. Int. Ed.* **2018**, *57*, 5156–5160. [CrossRef]
111. Ahmad, M.Z.; Navarro, M.; Lhotka, M.; Zornoza, B.; Téllez, C.; de Vos, W.M.; Benes, N.E.; Konnertz, N.M.; Visser, T.; Semino, R.; et al. Enhanced gas separation performance of 6FDA-DAM based mixed matrix membranes by incorporating MOF UiO-66 and its derivatives. *J. Membr. Sci.* **2018**, *558*, 64–77. [CrossRef]
112. Cheng, Y.; Tavares, S.R.; Doherty, C.M.; Ying, Y.; Sarnello, E.; Maurin, G.; Hill, M.R.; Li, T.; Zhao, D. Enhanced polymer crystallinity in mixed-matrix membranes induced by metal–organic framework nanosheets for efficient CO_2 Capture. *ACS Appl. Mater. Interfaces* **2018**, *10*, 43095–43103. [CrossRef] [PubMed]
113. Bachman, J.E.; Smith, Z.P.; Li, T.; Xu, T.; Long, J.R. Enhanced ethylene separation and plasticization resistance in polymer membranes incorporating metal–organic framework nanocrystals. *Nat. Mater.* **2016**, *15*, 845. [CrossRef] [PubMed]



© 2019 by the authors. Licensee MDPI, Basel, Switzerland. This article is an open access article distributed under the terms and conditions of the Creative Commons Attribution (CC BY) license (http://creativecommons.org/licenses/by/4.0/).